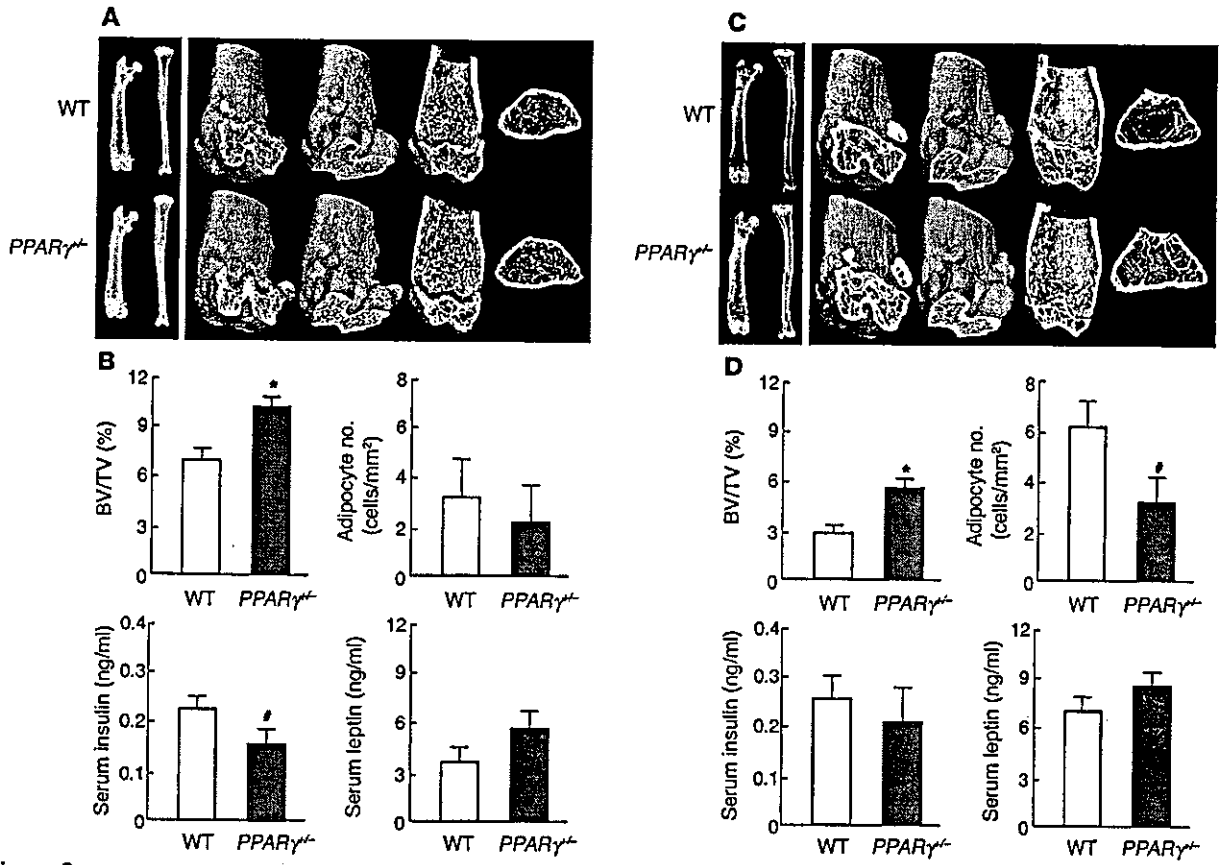

Figure 2

Radiological analysis and blood chemistry of heterozygous *PPARγ*-deficient (*PPARγ*$^{+/-}$) and WT littermates at 8 weeks (**A** and **B**) and 52 weeks (**C** and **D**) of age. (**A** and **C**) Plain x-ray images of femora and tibiae (left) and three-dimensional CT images of distal femora (right) of representative *PPARγ*$^{+/-}$ and WT littermates. (**B** and **D**) Trabecular BV expressed as percentage of total tissue volume (BV/TV [%]) at the distal femora was measured on the CT image. The number of adipocytes in the bone marrow, measured histologically, is shown here for collation with the BV/TV data. Insulin and leptin levels in serum taken just before the sacrifice were quantified using immunoassay kits. Data are expressed as means (bars) ± SEMs (error bars) for eight mice per group for *PPARγ*$^{+/-}$ and WT mice. Significant difference from WT: $^{*}P < 0.01$, $^{\#}P < 0.05$.

the cultures of ES cells between *PPARγ*$^{-/-}$ and WT (WT or *PPARγ*$^{+/+}$) genotypes isolated from blastocysts generated by mating *PPARγ*$^{+/-}$ mice (Figure 1A). In the presence of troglitazone, a thiazolidinedione that is a potent ligand of PPARγ, a substantial amount of oil red O–positive adipocytes was formed from WT ES cells, whereas adipogenesis was not seen in the *PPARγ*$^{-/-}$ ES cell culture (Figure 1A, upper row of photographs). To confirm the direct association between PPARγ and adipogenesis, PPARγ was reintroduced into *PPARγ*$^{-/-}$ ES cells using a retrovirus vector carrying the *PPARγ* gene (Rx-*PPARγ*). Adipogenesis was restored to the level similar to that of WT culture, although introduction of the same retrovirus vector without the *PPARγ* gene (Rx-vector) did not affect it. We then examined the osteogenesis in the *PPARγ*$^{-/-}$ and WT ES cell cultures. Surprisingly, in DMEM/10% FBS without osteogenic supplements such as dexamethasone, β-glycerophosphate, ascorbic acid, or BMP, the formation of von Kossa–positive bone nodules was potently induced in the *PPARγ*$^{-/-}$ ES cell culture, while this was not seen at all in the WT culture (Figure 1A, lower row of photographs). Quantitative analysis of the mRNA levels by the real-time RT-PCR method revealed that the marker genes for osteoblasts — type I collagen α1 chain (COL1A1), osteocalcin, and Runx2 — were upregulated in the *PPARγ*$^{-/-}$ ES cell culture as compared with the WT culture (Figure 1B). Reintroduction of PPARγ into the *PPARγ*$^{-/-}$ culture by Rx-*PPARγ* significantly decreased the nodule formation and osteogenic marker gene expressions, while the control Rx-vector altered neither (Figure 1, A and B). When one takes these results together, the observed mirror image regulations between adipogenesis and osteogenesis by loss and gain of the PPARγ function suggest a switching mechanism between the two differentiation pathways from common progenitors through the PPARγ signaling.

PPARγ haploinsufficiency leads to high bone mass in vivo. To learn the effect of the PPARγ insufficiency in vivo, we analyzed the bones of *PPARγ*$^{+/-}$ mice because the homozygous deficient fetuses died too early for their skeletal analyses to be performed. *PPARγ*$^{+/-}$ mice showed normal weight gain without visible general lipodystrophy on a standard diet during the observation period of up to 52 weeks of age. The lengths of the trunk and long bones were also similar to those of WT littermates, indicating that PPARγ is not involved in the regulation of skeletal growth. X-ray and three-dimensional CT analyses of femora and tibiae, however, revealed that *PPARγ*$^{+/-}$ mice showed about 40% higher trabecular bone mass than WT littermates at 8 weeks of age (Figure 2, A and B).

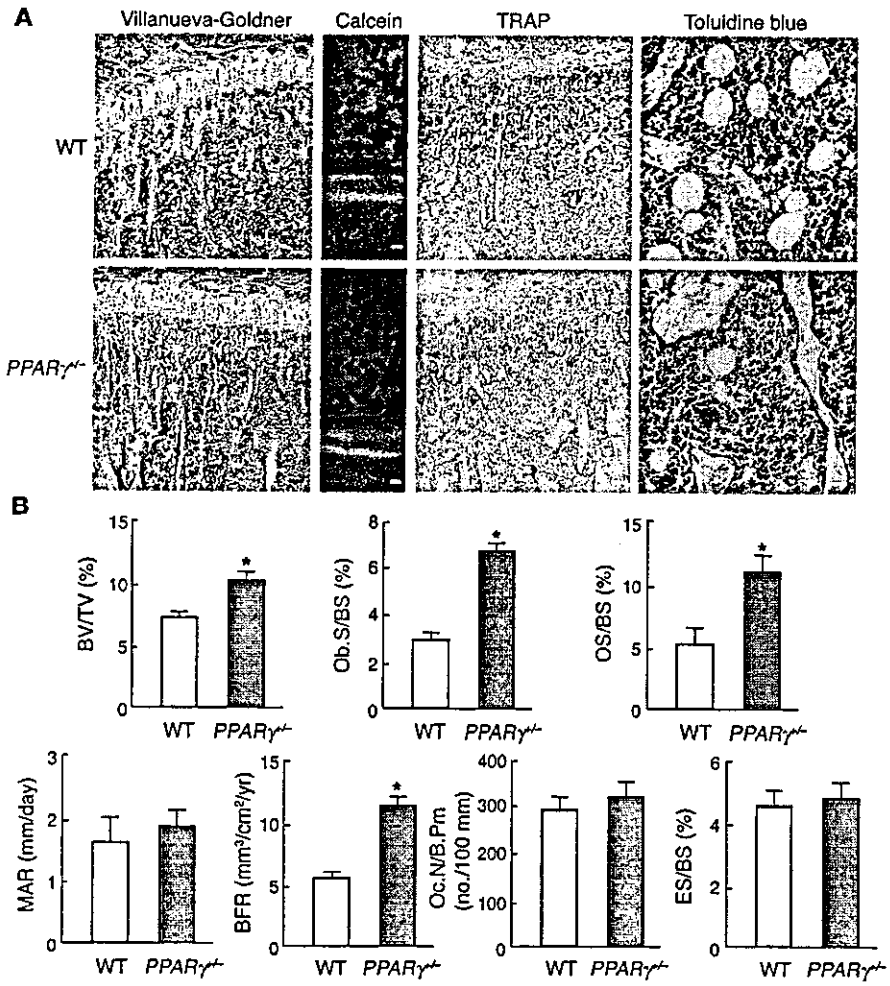

Figure 3
Histological analysis of the proximal tibiae of *PPARγ*$^{+/-}$ and WT littermates. (**A**) Histological features at proximal tibiae of *PPARγ*$^{+/-}$ and WT littermates. Villanueva-Goldner staining, calcein double labeling, and TRAP staining were done at 8 weeks; toluidine blue staining was done at 52 weeks of age. In Villanueva-Goldner staining, mineralized bone is stained green and unmineralized bone osteoid red; scale bar: 100 μm. In calcein double labeling, the mineralization front is stained as a green line; scale bar: 10 μm. In TRAP staining, TRAP-positive osteoclasts are stained red; scale bar: 100 μm. In toluidine blue staining, adipocytes are observed as oval vacuoles; scale bar: 50 μm. (**B**) Histomorphometric parameters at 8 weeks of age. Ob.S/BS, percentage of bone surface covered by cuboidal osteoblasts; OS/BS, percentage of bone surface covered by osteoid; MAR, mineral apposition rate; BFR, bone formation rate expressed by MAR times percentage of bone surface exhibiting double labels plus one-half single labels; Oc.N/B.Pm, number of mature osteoclasts in 100 mm of bone perimeter; ES/BS, percentage of eroded surface. Data are expressed as means (bars) ± SEMs (error bars) for eight mice per group for *PPARγ*$^{+/-}$ and WT mice. *Significant difference from WT, $P < 0.01$.

Contrarily, the number of adipocytes in the bone marrow determined as described below tended to be lower in the *PPARγ*$^{+/-}$ long bones compared with WT (Figure 2B). Similar changes of bone and fat were also seen in vertebral bodies (data not shown). To examine the involvement of systemic factors that are known to be related to bone and fat metabolism, the serum levels of insulin and leptin were compared between the two mouse genotypes. *PPARγ*$^{+/-}$ mice showed lower, although not significantly lower, serum insulin level and higher leptin level than WT littermates as reported previously (22, 29). Since insulin is known to be osteogenic (30), whereas leptin is antiosteogenic (11, 13, 31), neither of the changes in these hormones could explain the increased bone mass in *PPARγ*$^{+/-}$ mice.

Because age-related osteoporosis is known to be accompanied by reciprocal increase of bone marrow adipocytes (7–9), we further compared the bones of *PPARγ*$^{+/-}$ and WT littermates at 52 weeks of age (Figure 2, C and D). The BV of femora and tibiae was decreased in both mouse genotypes at this age as compared with that at 8 weeks; however, the difference of BV between *PPARγ*$^{+/-}$ and WT became more prominent at 52 weeks than at 8 weeks (95% versus 40%, respectively). The number of bone marrow adipocytes, which are shown as oval vacuoles by the toluidine blue staining (Figure 3A, right), was significantly decreased in *PPARγ*$^{+/-}$ mice at this age. This tendency was similarly observed in vertebral bodies (data not shown). Both insulin and leptin levels at this old age showed patterns similar to those at 8 weeks, although significant differences between the genotypes were not seen.

PPARγ haploinsufficiency leads to osteoblastogenesis in vivo. We further performed histological analyses of the proximal tibiae of 8-week-old *PPARγ*$^{+/-}$ mice. Villanueva-Goldner staining indicated increases of trabecular bones stained in green and osteoid surface stained in red in *PPARγ*$^{+/-}$ mice as compared with WT littermates; however, bone formation by individual osteoblasts determined by the calcein double labeling and the number of TRAP-positive osteoclasts was similar for the two groups (Figure 3A). Bone histomorphometric analyses (Figure 3B) confirmed the increase of BV by PPARγ haploinsufficiency to be about 40%. Among bone formation parameters, osteoblast surface and osteoid surface, both representative of the number of osteoblasts, were more than double in *PPARγ*$^{+/-}$ than in WT littermates, while the mineral apposition rate that reflects the bone formation ability of individual osteoblasts did not differ between them. Consequently, bone formation rate that is determined by the number and the function of osteoblasts became about twice that by PPARγ haploinsufficiency. Bone resorption parameters, osteoclast number, and eroded surface did not differ between *PPARγ*$^{+/-}$ and WT mice. Taking these histologi-

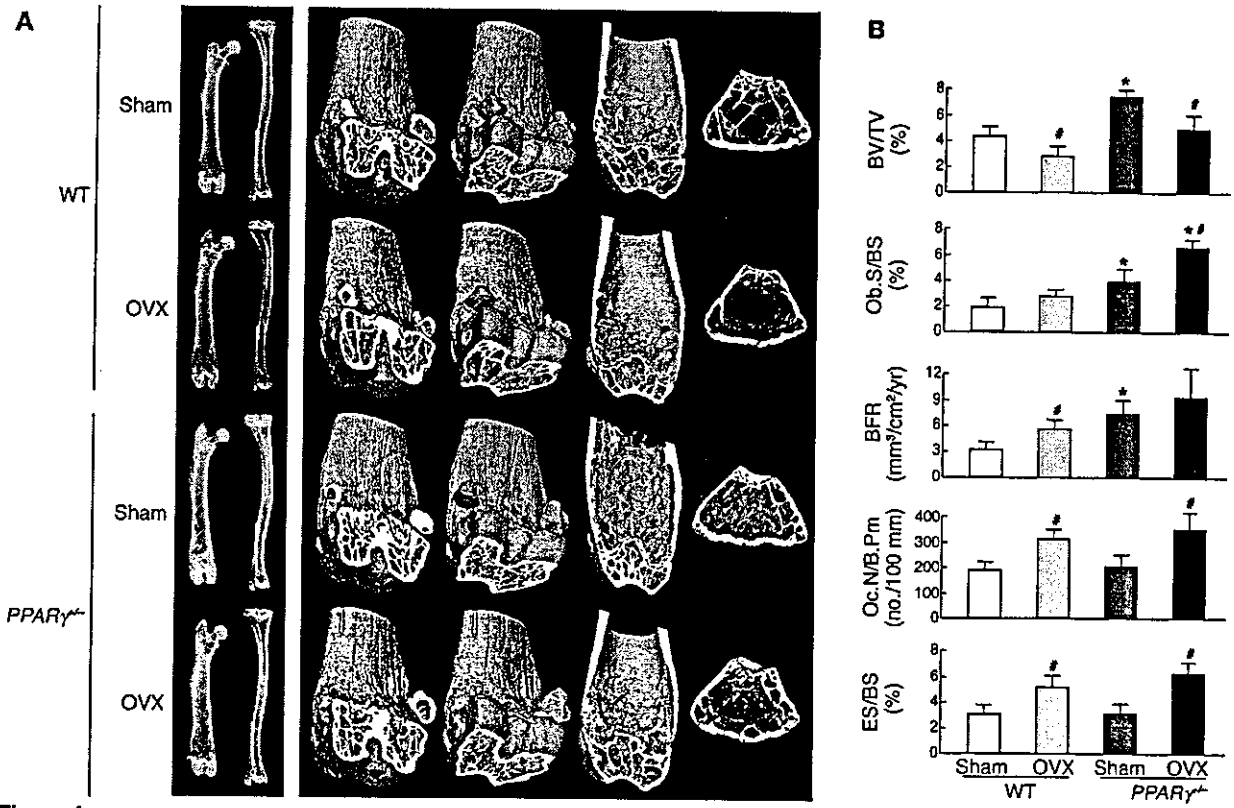

Figure 4

Radiological and histomorphometric analyses of OVX and sham-operated (Sham) female littermates of *PPARγ*$^{+/-}$ and WT genotypes. Female mice underwent surgical operation at 26 weeks and were analyzed at 30 weeks of age. (**A**) Plain x-ray images of femora and tibiae (left) and three-dimensional CT images of distal femora (right) of representative mice. (**B**) Histomorphometric parameters. Data are expressed as means (bars) ± SEMs (error bars) for eight mice per group for *PPARγ*$^{+/-}$ and WT mice. *Significant difference from WT, $P < 0.01$. #Significant difference from sham, $P < 0.05$.

cal observations together, *PPARγ*$^{+/-}$ mice exhibited high bone mass with increased osteoblastogenesis but normal osteoblast and osteoclast functions. The thickness of the growth plate at the proximal tibiae was not different between *PPARγ*$^{+/-}$ and WT littermates (80.4 ± 9.6 and 82.7 ± 10.3 μm, mean ± SEM of eight mice each, respectively), confirming that PPARγ signaling is not important for bone growth through chondrocyte functions.

PPARγ haploinsufficiency does not affect bone loss by OVX. To investigate the involvement of the PPARγ signaling in the mechanism of bone loss by estrogen deficiency, OVX or sham operation was undertaken on 26-week-old female *PPARγ*$^{+/-}$ and WT littermates, and BV was compared 4 weeks after the operation. X-ray and three-dimensional CT analyses of femora and tibiae suggested that both *PPARγ*$^{+/-}$ and WT mice showed similar bone loss by OVX (Figure 4A). Histomorphometric analyses (Figure 4B) showed that BV was about 30% decreased by OVX in both *PPARγ*$^{+/-}$ and WT mice. These decreases were accompanied by increases in bone formation and bone resorption parameters, indicating a state of high bone turnover, in both genotypes. Hence, PPARγ haploinsufficiency did not affect the change of bone metabolism induced by OVX, suggesting that the PPARγ signaling does not contribute to osteopenia caused by estrogen deficiency.

PPARγ haploinsufficiency leads to osteoblastogenesis from cultured bone marrow cells. To investigate the cellular mechanism underlying the abnormality in the bone of *PPARγ*$^{+/-}$ mice, ex vivo cultures of bone marrow cells derived from long bones were performed. We first compared the cell proliferation determined by the growth curve for 4 days and found no difference between *PPARγ*$^{+/-}$ and WT marrow cells (Figure 5A). Adipogenesis from marrow cells in the presence of troglitazone was confirmed to be inhibited by PPARγ haploinsufficiency, however, since the number of oil red O-positive adipocytes was decreased in the *PPARγ*$^{+/-}$ culture to about half that of the WT culture (Figure 5B). We further examined osteoblastogenesis in the bone marrow cell culture by comparing the numbers of colonies positively stained with ALP, Alizarin red S, and von Kossa (Figure 5C). All colonies were markedly increased in the *PPARγ*$^{+/-}$ culture as compared with the WT culture, indicating the increase of osteoblastogenesis from bone marrow progenitors by PPARγ haploinsufficiency.

To further investigate the regulation of expression of genes related to bone metabolism by PPARγ haploinsufficiency, we compared mRNA levels of key or marker molecules for adipocyte and osteoblast differentiations between *PPARγ*$^{+/-}$ and WT bone marrow cells (Figure 5D). As expected, PPARγ expression was reduced in the *PPARγ*$^{+/-}$ marrow cells compared with the WT. The levels of expression of other key factors for adipocyte differentiation, C/EBP-β and C/EBP-δ, in the *PPARγ*$^{+/-}$ marrow cells were comparable to those of WT, indicating that PPARγ was not essential for induction of these C/EBPs; contrarily, C/EBP-α was significantly reduced. Based on previous observations (16, 17, 22, 32, 33) and these results, it appears that C/EBP-β and C/EBP-δ lie upstream of PPARγ, while C/EBP-α is

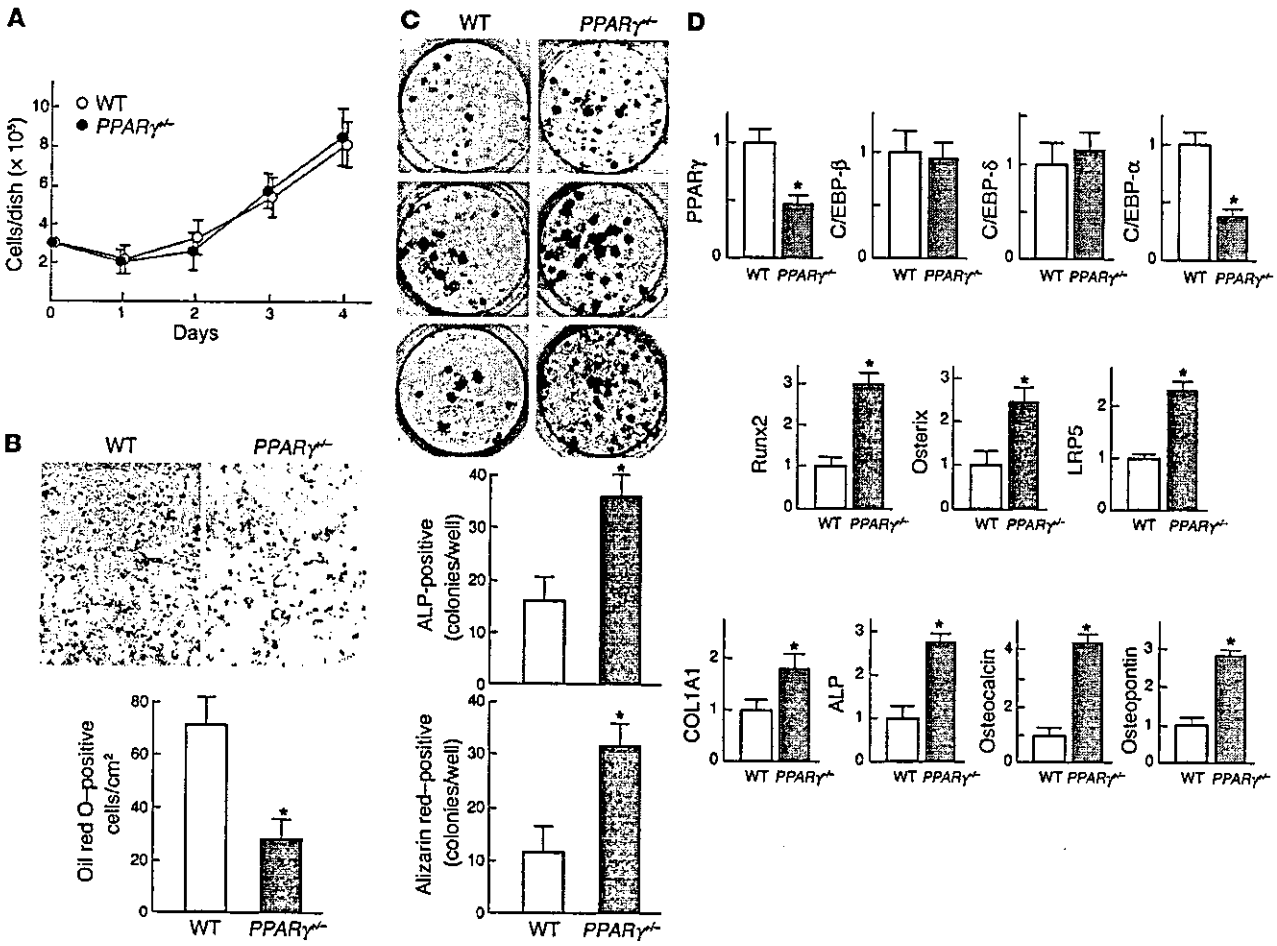

Figure 5

Adipogenesis and osteogenesis in the cultures of bone marrow cells from *PPARγ*$^{-/-}$ and WT littermates. (**A**) Growth curves of bone marrow cells isolated from *PPARγ*$^{-/-}$ and WT mice. The adherent bone marrow cells were inoculated at a density of 3×10^5 cells/dish in 10-cm culture dishes. The cells per dish were counted at 1, 2, 3, and 4 days of culture. Data are expressed as means (symbols) ± SEMs (error bars) for eight dishes per group. (**B**) Adipogenesis determined by oil red O staining in the culture of bone marrow cells in α-MEM/10% FBS with troglitazone. The graph indicates the number of positive cells per square centimeter. (**C**) Osteogenesis determined by ALP (upper row), Alizarin red (middle row), and von Kossa (lower row) stainings in the culture of bone marrow cells in α-MEM/10% FBS with ascorbic acid and β-glycerophosphate. The graphs below indicate the number of ALP-positive (upper) and Alizarin red–positive (lower) colonies per well. Data are expressed as means (bars) ± SEMs (error bars) for eight wells per group (**B** and **C**). *Significant difference from the WT culture, $P < 0.01$. (**D**) Expression of key molecules for adipogenesis (PPARγ, C/EBP-β, C/EBP-δ, and C/EBP-α) and osteogenesis (Runx2, osterix, and LRP5), and marker proteins for osteogenesis (COL1A1, ALP, osteocalcin, and osteopontin) determined by quantitative RT-PCR in the bone marrow cells at 14 days of culture under the conditions above. The ordinate axis indicates the relative amount of mRNA as compared with that of WT.

regulated, at least in part, downstream of PPARγ. Regarding osteogenic factors, expressions of the putative central determinants of major pathways for osteoblast differentiation, Runx2 (34), osterix (35), and LDL receptor-related protein 5 (LRP5) (36), were increased in the *PPARγ*$^{-/-}$ culture as compared with WT, indicating that the PPARγ signaling directly or indirectly impacts these major pathways for osteoblast differentiation. Expressions of matrix proteins representing osteogenesis, COL1A1, ALP, osteocalcin, and osteopontin, were also higher in the *PPARγ*$^{-/-}$ culture than in the WT culture, which was consistent with the in vivo histomorphometric data showing high bone mass with increased osteoblastogenesis.

When we examined the proliferation, differentiation, and matrix synthesis of cultured calvarial osteoblasts, which we confirmed to be more mature than bone marrow cells, none of them showed a difference between *PPARγ*$^{-/-}$ and WT mice (data not shown). This indicates that PPARγ haploinsufficiency affects only marrow progenitors, but not cells that are more committed to osteoblastic lineage. Furthermore, studies using the coculture system of marrow cells/calvarial osteoblasts and the M-BMMϕ culture system (28, 37) also failed to show difference of differentiation, bone-resorbing activity, or survival of the osteoclastic cells, suggesting that PPARγ is not important for osteoclast functions.

Discussion

Osteoblastogenesis was upregulated not only in the *PPARγ*$^{-/-}$ bone in vivo, but also in the cultures of *PPARγ*$^{-/-}$ ES cells and *PPARγ*$^{+/-}$

primary bone marrow cells. Considering that the former culture was performed in the absence of any osteogenic stimulation, under which condition no WT stem cells can differentiate into osteoblasts, the intrinsic PPARγ signaling seems to function as a potent suppressor of commitment and differentiation to the osteoblastic lineage. Its molecular mechanism remains unclear, however. A previous report showed that a stable transfection of PPARγ and its activation with a thiazolidinedione-suppressed Runx2, type I collagen, and osteocalcin syntheses in the culture of a stromal cell line (38). Although the present study also showed that steady-state mRNA levels of the key molecules for osteoblast differentiation, Runx2, osterix, and LRP5, were upregulated in primary cultured marrow cells with PPARγ haploinsufficiency (Figure 5D), whether this is transcriptional regulation or secondary to the increase in cells of osteoblast lineage in the culture is unknown. The predicted region of the PPARγ-responsive element PPRE (TGACCTnTGACCT) has not been identified in the promoter of these genes and was not found by our genomic search, at least in the region between 4.0 kb upstream and 0.5 kb downstream of the transcriptional start point of *runx2* (GenBank accession number NT 039655), *osterix* (NT 039621), and *lrp5* (NT 039684) genes. It should, however, also be noted that several reports have indicated that PPARγ regulates gene expression independently of PPRE, that is, by interfering with the function of AP-1, signal transducer and activator of transcription 1 (STAT1), and NF-κB (39), or by inhibiting the function of GHP-1, a transcription factor implicated in pituitary-specific gene expression (40). The AP-1 family members may possibly play a role in the mechanism, especially for mesenchymal cells. Activation of PPARγ is reported to suppress *c-fos* expression (41). Another AP-1 family member, DeltaFosB, is known to be a positive regulator of osteoblast differentiation, and the transgenic mouse leads to postnatal high bone mass with increased osteoblastogenesis and decreased adipogenesis in bone marrow (12). Another possible molecular mechanism is the interaction of PPARγ with the TGF-β/Smad3 signaling, which inhibits osteoblast differentiation (42, 43). Since Smad3 is reported to interact physically with Runx2 (42) and PPARγ (44), the interference by PPARγ with the Smad3 inhibition of Runx2 might be involved in the switching mechanism between adipocyte and osteoblast differentiation. The interaction of PPARγ with Wnt signaling might be another issue to pursue. The canonical Wnt pathway, likely mediated by Wnt10b, is known to maintain preadipocytes in an undifferentiated state through stabilization of cytosolic β-catenin (45, 46). Since activation of PPARγ with troglitazone is not sufficient to repress expression of Wnt10b, Wnt signaling might lie upstream of PPARγ. Recently, in addition to LRP5, which is a coreceptor of Wnt, the canonical Wnt-signaling molecules β-catenin and glycogen synthase kinase-3β have been reported to stimulate osteoblast differentiation (47, 48), indicating a switching between adipogenesis and osteogenesis by the Wnt signaling. Further studies on functional interaction of PPARγ with the transcriptional and signaling molecules above will elucidate the switching mechanism between the two differentiation pathways from common progenitors.

PPARγ may also inhibit osteogenesis indirectly through its stimulation of adipogenesis from marrow progenitors that can give rise to either osteoblasts or adipocytes. In fact, many experimental models have provided substantial evidence for this reciprocal relationship between cell lineages (6, 10–15), and there is little doubt that adipogenesis increases as BV decreases, suggesting that marrow adipogenesis has important implications in osteogenic disorders (7–9). Evidence of the transdifferentiation of stromal cells actually suggests a large degree of plasticity between osteoblasts and adipocytes (4, 49), although it is not clear at what point the phenotype of these multipotential cells becomes committed to either osteoblast or adipocyte differentiation. Since differentiated osteoblasts indicated by osteocalcin expression are reported to undergo adipogenic differentiation (4), it is possible that the reciprocal relationship between osteogenesis and adipogenesis may, at least in part, be due to the transdifferentiation between rather differentiated cells of the two lineages. To determine the role of PPARγ in more differentiated osteoblastic cells than bone marrow cells, we used calvarial cells whose spontaneous differentiation is known to follow not only the osteogenic pathway but also the adipogenic pathway (49). Despite the existence of PPARγ expression in these cells as well, its haploinsufficiency did not affect the cell functions, suggesting that PPARγ signaling may be involved in the earlier, but not the later, stage of relationship between the two cell lineages.

Hormones regulating bone and fat metabolisms include insulin and leptin, both of which are known to be related to the PPARγ signaling. Insulin is known to play important anabolic roles in bone (30), and deficiency of insulin signaling is associated with osteopenia both in mice and humans (27, 50–52). A series of reports demonstrated that leptin, a well-known anorexigenic hormone secreted by adipocytes (53), also shows antiosteogenic action centrally through the hypothalamic and sympathetic nervous systems (11, 13, 31). In the present study, neither insulin nor leptin seemed to mediate the high bone mass in *PPARγ*$^{+/-}$ mice, since the serum levels of these hormones were, quite unexpectedly, the opposite of those causing osteogenic functions. PPARγ activation is known to cause insulin sensitivity, thus *PPARγ*$^{+/-}$ mice were assumed to develop insulin resistance; however, the serum insulin level was normal or somewhat decreased as previously reported (22, 29). This appears, at least in part, due to hypersecretion of leptin, which was also unexpected, given that the marrow adipocytes, a positive regulator of leptin expression, were decreased in *PPARγ*$^{+/-}$ mice. Our previous studies clearly demonstrated that cultured primary adipocytes from *PPARγ*$^{+/-}$ mice expressed and secreted increased levels of leptin as compared with those from WT (22, 29). In this respect, since leptin is known to have a functional PPRE whose activity is suppressed by PPARγ activation in adipocytes (54, 55), it is likely that the increased level of leptin is due to a partial release from the suppressive effect of PPARγ on leptin gene transcription by loss of one *PPARγ* allele.

Age-related bone loss has been suggested to be attributable to increased adipogenesis at the expense of osteoblastogenesis (7–9). Indeed, studies of SAMP6 mice, a murine model of age-related osteopenia, have established a tight association between osteopenia and enhanced adipogenesis (10, 15). The fact that the effects of PPARγ haploinsufficiency on both the increase in bone volume and the decrease in adipocytes were stronger at 52 weeks than at 8 weeks suggests the involvement of the PPARγ signaling in the pathophysiology of human age-related osteoporosis. In fact, our preliminary examination of the bone marrow specimen from patients with femoral neck fracture actually showed increases of both the PPARγ mRNA level and fat mass in older patients (data not shown) as compared with those in younger patients, although the causality between PPARγ level and adipogenesis remains unknown since adipocytes can be both the source and the target

of PPARγ. An association study between bone density and a genetic polymorphism of *PPARγ* in postmenopausal women implies the involvement of PPARγ in bone loss, although the functional relevance remains unclear (56). We should, however, keep in mind that there are two distinct factors that determine involutional osteoporosis: a rapid bone loss after menopause as a result of estrogen withdrawal and a gradual age-related bone loss thereafter (57). From the present study showing that PPARγ insufficiency did not affect bone loss by OVX, PPARγ may not be involved in the former stage, but may play a role in the latter. To confirm the involvement of PPARγ in human osteoporosis, the next task ahead of us will be to perform a genetic association study with stratified analysis by age and menopausal state, and more importantly, to use a cohort population.

We conclude herein that PPARγ haploinsufficiency leads to the increase of bone mass by stimulating osteoblastogenesis from bone marrow progenitors without affecting differentiated osteoblasts or osteoclast lineage cells. Based on the present and previous evidence presented, we believe that PPARγ may be a novel target for therapeutic intervention of osteopenic disorders, although the mechanism remains to be clarified. Appropriate functional antagonism of PPARγ may provide a potentially novel approach to increasing bone formation and therefore, as a stand-alone therapy or in combination with an antiresorptive medication, may provide more efficacious prevention or treatment of osteoporosis.

Acknowledgments

We thank the hard tissue research team at Kureha Chemical Co. for technical assistance. We are grateful to Bruce M. Spiegelman for the pBabe-mPPARγ2-puro vector. This work was supported by Grants-in-Aid for Scientific Research from the Japanese Ministry of Education, Culture, Sports, Science, and Technology (1370303) and the ONO Medical Research Foundation.

Received for publication August 28, 2003, and accepted in revised form January 6, 2004.

Address correspondence to: Hiroshi Kawaguchi, Department of Orthopaedic Surgery, Faculty of Medicine, University of Tokyo, Hongo 7-3-1, Bunkyo-ku, Tokyo 113-8655, Japan. Phone: 81-33815-5411 ext. 30473 or 33376; Fax: 81-33818-4082; E-mail: kawaguchi-ort@h.u-tokyo.ac.jp.

1. Beresford, J.N. 1989. Osteogenic stem cells and the stromal system of bone and marrow. *Clin. Orthop.* 240:270–280.
2. Pittenger, M.F., et al. 1999. Multilineage potential of adult human mesenchymal stem cells. *Science.* 284:143–147.
3. Bennett, J.H., Joyner, C.J., Triffitt, J.T., and Owen, M.E. 1991. Adipocytic cells cultured from marrow have osteogenic potential. *J. Cell Sci.* 99:131–139.
4. Nuttall, M.E., Patton, A.J., Olivera, D.L., Nadeau, D.P., and Gowen, M. 1998. Human trabecular bone cells are able to express both osteoblastic and adipocytic phenotype: implications for osteopenic disorders. *J. Bone Miner. Res.* 13:371–382.
5. Park, S.R., Oreffo, R.O., and Triffitt, J.T. 1999. Interconversion potential of cloned human marrow adipocytes in vitro. *Bone.* 24:549–554.
6. Beresford, J.N., Bennett, J.H., Devlin, C., Leboy, P.S., and Owen, M.E. 1992. Evidence for an inverse relationship between the differentiation of adipocytic and osteogenic cells in rat marrow stromal cell cultures. *J. Cell Sci.* 102:341–351.
7. Meunier, P., Aaron, J., Edouard, C., and Vignon, G. 1971. Osteoporosis and the replacement of cell populations of the marrow by adipose tissue. A quantitative study of 84 iliac bone biopsies. *Clin. Orthop.* 80:147–154.
8. Burkhardt, R., et al. 1987. Changes in trabecular bone, hematopoiesis and bone marrow vessels in aplastic anemia, primary osteoporosis, and old age: a comparative histomorphometric study. *Bone.* 8:157–164.
9. Rozman, C., et al. 1989. Age-related variations of fat tissue fraction in normal human bone marrow depend both on size and number of adipocytes: a stereological study. *Exp. Hematol.* 17:34–37.
10. Jilka, R.L., Weinstein, R.S., Takahashi, K., Parfitt, A.M., and Manolagas, S.C. 1996. Linkage of decreased bone mass with impaired osteoblastogenesis in a murine model of accelerated senescence. *J. Clin. Invest.* 97:1732–1740.
11. Ducy, P., et al. 2000. Leptin inhibits bone formation through a hypothalamic relay: a central control of bone mass. *Cell.* 100:197–207.
12. Sabatakos, G., et al. 2000. Overexpression of DeltaFosB transcription factor(s) increases bone formation and inhibits adipogenesis. *Nat. Med.* 6:985–990.
13. Takeda, S., et al. 2002. Leptin regulates bone formation via the sympathetic nervous system. *Cell.* 111:305–317.
14. Takeuchi, Y., et al. 2002. Interleukin-11 as a stimulatory factor for bone formation prevents bone loss with advancing age in mice. *J. Biol. Chem.* 277:49011–49018.
15. Kodama, Y., et al. 1998. Reduced expression of interleukin-11 in bone marrow stromal cells of senescence-accelerated mice (SAMP6): relationship to osteopenia with enhanced adipogenesis. *J. Bone Miner. Res.* 13:1370–1377.
16. Rosen, E.D., Walkey, C.J., Puigserver, P., and Spiegelman, B.M. 2000. Transcriptional regulation of adipogenesis. *Genes Dev.* 14:1293–1307.
17. Rosen, E.D., and Spiegelman, B.M. 2001. PPARγ: a nuclear regulator of metabolism, differentiation, and cell growth. *J. Biol. Chem.* 12:37731–37734.
18. Kersten, S., Desvergne, B., and Wahli, W. 2000. Roles of PPARs in health and disease. *Nature.* 405:421–424.
19. Mangelsdorf, D.J., and Evans, R.M. 1995. The RXR heterodimers and orphan receptors. *Cell.* 83:841–850.
20. Tontonoz, P., Hu, E., and Spiegelman, B.M. 1994. Stimulation of adipogenesis in fibroblasts by PPAR γ 2, a lipid-activated transcription factor. *Cell.* 79:1147–1156.
21. Barak, Y., et al. 1999. PPAR γ is required for placental, cardiac, and adipose tissue development. *Mol. Cell.* 4:585–595.
22. Kubota, N., et al. 1999. PPAR γ mediates high-fat diet-induced adipocyte hypertrophy and insulin resistance. *Mol. Cell.* 4:597–609.
23. Rosen, E.D., et al. 1999. PPAR γ is required for the differentiation of adipose tissue in vivo and in vitro. *Mol. Cell.* 4:611–617.
24. Kadowaki, T. 2000. Insights into insulin resistance and type 2 diabetes from knockout mouse models. *J. Clin. Invest.* 106:459–465.
25. Bradley, A. 1987. Production and analysis of chimaeric mice. In *Teratocarcinomas and embryonic stem cells.* E.J. Robertson, editor. IRL Press. Oxford, United Kingdom. 113–151.
26. Keller, G.M. 1995. In vitro differentiation of embryonic stem cells. *Curr. Opin. Cell Biol.* 7:862–869.
27. Akune, T., et al. 2002. Insulin receptor substrate-2 maintains predominance of anabolic function over catabolic function of osteoblasts. *J. Cell Biol.* 159:147–156.
28. Kobayashi, K., et al. 2000. Tumor necrosis factor α stimulates osteoclast differentiation by a mechanism independent of the ODF/RANKL-RANK interaction. *J. Exp. Med.* 191:275–286.
29. Yamauchi, T., et al. 2001. The mechanisms by which both heterozygous peroxisome proliferator-activated receptor γ (PPARγ) deficiency and PPARgamma agonist improve insulin resistance. *J. Biol. Chem.* 276:41245–41254.
30. Thomas, D.M., Hards, D.K., Rogers, S.D., Ng, K.W., and Best, J.D. 1997. Insulin and bone, clinical and scientific view. *Endocrinology and Metabolism.* 4:5–17.
31. Takeda, S., and Karsenty, G. 2001. Central control of bone formation. *J. Bone Miner. Metab.* 19:195–198.
32. Tanaka, T., Yoshida, N., Kishimoto, T., and Akira, S. 1997. Defective adipocyte differentiation in mice lacking the C/EBPβ and/or C/EBPδ gene. *EMBO J.* 16:7432–7443.
33. Wu, Z., et al. 1999. Cross-regulation of C/EBP α and PPAR γ controls the transcriptional pathway of adipogenesis and insulin sensitivity. *Mol. Cell.* 3:151–158.
34. Karsenty, G. 2001. Minireview: transcriptional control of osteoblast differentiation. *Endocrinology.* 142:2731–2733.
35. Nakashima, K., et al. 2002. The novel zinc finger-containing transcription factor osterix is required for osteoblast differentiation and bone formation. *Cell.* 108:17–29.
36. Patel, M.S., and Karsenty, G. 2002. Regulation of bone formation and vision by LRP5. *N. Engl. J. Med.* 346:1572–1574.
37. Suda, T., et al. 1999. Modulation of osteoclast differentiation and function by the new members of the tumor necrosis factor receptor and ligand families. *Endocr. Rev.* 20:345–357.
38. Lecka-Czernik, B., et al. 1999. Inhibition of Osf2/Cbfa1 expression and terminal osteoblast differentiation by PPARγ2. *J. Cell. Biochem.* 74:357–371.
39. Ricote, M., Li, A.C., Willson, T.M., Kelly, C.J., and Glass, C.K. 1998. The peroxisome proliferator-activated receptor-γ is a negative regulator of macrophage activation. *Nature.* 391:79–82.
40. Tolon, R.M., Castillo, A.I., and Aranda, A. 1998. Activation of the prolactin gene by peroxisome proliferator-activated receptor-α appears to be DNA binding-independent. *J. Biol. Chem.* 273:26652–26661.
41. Benson, S., Wu, J., Padmanabhan, S., Kurtz, T.W., and Pershadsingh, H.A. 2000. Peroxisome proliferator-activated receptor (PPAR)-γ expression in human vascular smooth muscle cells: inhibition of growth, migration, and c-fos expression by the peroxisome proliferator-activated receptor (PPAR)-γ activator troglitazone. *Am. J. Hypertens.* 13:74–82.
42. Alliston, T., Choy, L., Ducy, P., Karsenty, G., and

Derynck, R. 2001. TGF-β-induced repression of CBFA1 by Smad3 decreases cbfa1 and osteocalcin expression and inhibits osteoblast differentiation. *EMBO J.* 20:2254–2272.
43. Borton, A.J., Frederick, J.P., Datto, M.B., Wang, X.P., and Weinstein, R.S. 2001. The loss of Smad3 results in a lower rate of bone formation and osteopenia through dysregulation of osteoblast differentiation and apoptosis. *J. Bone Miner. Res.* 16:1754–1764.
44. Fu, M., et al. 2001. Peroxisome proliferator-activated receptor γ inhibits transforming growth factor beta-induced connective tissue growth factor expression in human aortic smooth muscle cells by interfering with Smad3. *J. Biol. Chem.* 276:45888–45894.
45. Ross, S.E., et al. 2000. Inhibition of adipogenesis by Wnt signaling. *Science.* 289:950–953.
46. Bennett, C.N., et al. 2002. Regulation of Wnt signaling during adipogenesis. *J. Biol. Chem.* 277:30998–31004.
47. Bain, G., Muller, T., Wang, X., and Papkoff, J. 2003. Activated β-catenin induces osteoblast differentiation of C3H10T1/2 cells and participates in BMP2 mediated signal transduction. *Biochem. Biophys. Res. Commun.* 301:84–91.
48. Smith, E., Coetzee, G.A., and Frenkel, B. 2002. Glucocorticoids inhibit cell cycle progression in differentiating osteoblasts via glycogen synthase kinase-3β. *J. Biol. Chem.* 277:18191–18197.
49. Garcia, T., et al. 2002. Behavior of osteoblast, adipocyte, and myoblast markers in genome-wide expression analysis of mouse calvaria primary osteoblasts in vitro. *Bone.* 31:205–211.
50. Krakauer, J.C., McKenna, M.J., Rao, D.S., and Whitehouse, F.W. 1997. Bone mineral density in diabetes. *Diabetes Care.* 20:1339–1340.
51. Piepkorn, B., et al. 1997. Bone mineral density and bone metabolism in diabetes mellitus. *Horm. Metab. Res.* 29:584–591.
52. Ogata, N., et al. 2000. Insulin receptor substrate-1 in osteoblast is indispensable for maintaining bone turnover. *J. Clin. Invest.* 105:935–943.
53. Elmquist, J.K., Elias, C.F., and Saper, C.B. 1999. From lesions to leptin: hypothalamic control of food intake and body weight. *Neuron.* 22:221–232.
54. Kallen, C.B., and Lazar, M.A. 1996. Antidiabetic thiazolidinediones inhibit leptin (ob) gene expression in 3T3-L1 adipocytes. *Proc. Natl. Acad. Sci. U. S. A.* 93:5793–5796.
55. Hollenberg, A.N., et al. 1997. Functional antagonism between CCAAT/enhancer binding protein-α and peroxisome proliferator-activated receptor-γ on the leptin promoter. *J. Biol. Chem.* 272:5283–5290.
56. Ogawa, S., et al. 1999. Association of bone mineral density with a polymorphism of the peroxisome proliferator-activated receptor γ gene: PPARγ expression in osteoblasts. *Biochem. Biophys. Res. Commun.* 260:122–126.
57. Nguyen, T.V., Blangero, J., and Eisman, J.A. 2000. Genetic epidemiological approaches to the search for osteoporosis genes. *J. Bone Miner. Res.* 15:392–401.

THE JOURNAL OF BIOLOGICAL CHEMISTRY

Vol. 279, No. 15, Issue of April 9, pp. 15314–15322, 2004
Printed in U.S.A.

Impairment of Bone Healing by Insulin Receptor Substrate-1 Deficiency*

Received for publication, November 16, 2003, and in revised form, January 15, 2004
Published, JBC Papers in Press, January 21, 2004, DOI 10.1074/jbc.M312525200

Takashi Shimoaka‡, Satoru Kamekura‡, Hirotaka Chikuda§, Kazuto Hoshi§, Ung-il Chung§, Toru Akune‡, Zenjiro Maruyama¶, Toshihisa Komori¶, Michihiro Matsumoto‖, Wataru Ogawa‖, Yasuo Terauchi, Takashi Kadowaki**, Kozo Nakamura‡, and Hiroshi Kawaguchi‡ ‡‡**

*From the Departments of ‡Orthopaedic Surgery, §Tissue Engineering, and **Metabolic Diseases, Faculty of Medicine, University of Tokyo, Hongo, Bunkyo, Tokyo 113-8655, ¶Department of Molecular Medicine, Osaka University Medical School, Suita, Osaka 565-0871, and ‖Division of Diabetes, Digestive and Kidney Diseases, Kobe University Graduate School of Medicine, Kobe 650-0017, Japan*

Insulin receptor substrate-1 (IRS-1) is an essential molecule for intracellular signaling of insulin-like growth factor (IGF)-I and insulin, both of which are potent anabolic regulators of bone and cartilage metabolism. To investigate the role of IRS-1 in bone regeneration, fracture was introduced in the tibia, and its healing was compared between wild-type (WT) mice and mice lacking the *IRS-1* gene (*IRS-1*$^{-/-}$ mice). Among 15 *IRS-1*$^{-/-}$ mice, 12 remained in a non-union state even at 10 weeks after the operation, whereas all 15 WT mice showed a rigid bone union at 3 weeks. This impairment was because of the suppression of callus formation with a decrease in chondrocyte proliferation and increases in hypertrophic differentiation and apoptosis. Reintroduction of IRS-1 to the *IRS-1*$^{-/-}$ fractured site using an adenovirus vector significantly restored the callus formation. In the culture of chondrocytes isolated from the mouse growth plate, *IRS-1*$^{-/-}$ chondrocytes showed less mitogenic ability and Akt phosphorylation than WT chondrocytes. An Akt inhibitor decreased the IGF-I-stimulated DNA synthesis of chondrocytes more potently in the WT culture than in the *IRS-1*$^{-/-}$ culture. We therefore conclude that IRS-1 deficiency impairs bone healing at least partly by inhibiting chondrocyte proliferation through the phosphatidylinositol 3-kinase/Akt pathway, and we propose that IRS-1 can be a target molecule for bone regenerative medicine.

In efforts to develop more advanced skeletal regenerative medicine through genetic manipulation, we have been attempting to identify genes implicated in bone and cartilage formation *in vivo*. Healing of bone fracture is composed of complex multistep processes involving a variety of cellular events for bone and cartilage regeneration (1, 2). Under the periosteum adjacent to the fracture gap, undifferentiated mesenchymal cells start differentiation directly to cells of osteoblastic lineage for the membranous ossification, whereas in granulation tissue inside the fracture gap, these mesenchymal cells undergo endochondral bone formation; they differentiate first into chondrocytes to form cartilage which is subsequently replaced by calcified tissues. The size and quality of fracture callus that determine the mechanical property of the fracture site are mostly dependent on the latter process. Because the endochondral bone formation also takes place in embryonic development and in skeletal growth after birth, understanding the molecular mechanism of fracture healing may not only help treat non-union and delayed union of fracture itself but also help advance bone regenerative medicine.

Insulin-like growth factor-I (IGF-I)[1] plays important roles in the anabolic regulation of bone and cartilage metabolism (3). Osteoblasts and chondrocytes produce this growth factor, express its receptor, and respond to it (3, 4). IGF-I appears essential for normal bone development because deletion of IGF-I or its receptor leads to a reduction in bone size at birth (5, 6). Clinically, patients with Laron syndrome caused by IGF-I deficiency exhibit growth retardation and osteoporosis (7). IGF-I is also reported to be expressed during fracture healing and to stimulate it, suggesting a role as an autocrine/paracrine factor potentiating bone regeneration (8, 9). Insulin also plays important roles in the anabolic regulation of bone and cartilage metabolism (10). Although the anabolic effect of insulin on bone may be primarily related to its ability to stimulate osteoblast proliferation, that on cartilage may involve the acceleration of chondrocyte differentiation (11, 12). Patients with insulin deficiency as exemplified by type 1 diabetes mellitus are associated with osteoporosis (13, 14). Diabetes has also been shown to impair fracture healing, which is restored by treatment with insulin in both humans and animals (2, 15, 16).

Both IGF-I and insulin initiate cellular responses by binding to distinct cell-surface receptor tyrosine kinases that regulate a variety of signaling pathways controlling metabolism, growth, and survival. Insulin receptor substrates (IRSs) are essential substrates of the receptor tyrosine kinases, which integrate the pleiotropic effects of IGF-I and insulin on cellular function (17, 18). The mammalian IRS family contains at least four members: ubiquitous IRS-1 and IRS-2, adipose tissue-predominant

* This work was supported by Grants-in-aid for Scientific Research from the Japanese Ministry of Education, Culture, Sports, Science and Technology 11470301 and 12137201, the Uehara Memorial Foundation, and the Takeda Science Foundation. The costs of publication of this article were defrayed in part by the payment of page charges. This article must therefore be hereby marked "*advertisement*" in accordance with 18 U.S.C. Section 1734 solely to indicate this fact.

‡‡ To whom correspondence should be addressed: Dept. of Orthopaedic Surgery, Faculty of Medicine, University of Tokyo, Hongo 7-3-1, Bunkyo, Tokyo 113-8655, Japan. Tel.: 81-3-3815-5411 (ext. 30473 or 33376); Fax: 81-3-3818-4082; E-mail: kawaguchi-ort@h.u-tokyo.ac.jp.

[1] The abbreviations used are: IGF, insulin-like growth factor; IRS, insulin receptor substrate; WT, wild-type; BMC, bone mineral content; HE, hematoxylin-eosin; PCNA, proliferating cell nuclear antigen; PBS, phosphate-buffered saline; TUNEL, terminal transferase dUTP nick end labeling; AxLacZ, adenovirus vector carrying β-galactosidase gene; DMEM, Dulbecco's modified Eagle's medium; PI3K, phosphatidylinositol 3-kinase; MAPK, mitogen-activated protein kinase; ERK, extracellular signal-regulated kinase; FGF, fibroblast growth factor; IGF-IR, insulin-like growth factor-I receptor; SHC, Src homology collagen; X-gal, 5-bromo-4-chloro-3-indolyl-β-D-galactopyranoside; FBS, fetal bovine serum; TdR, [^{3}H]thymidine; PI3K, phosphatidylinositol 3-kinase.

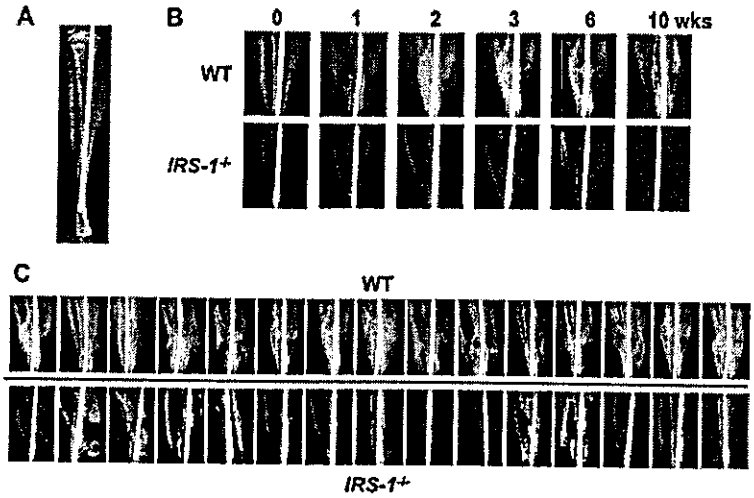

FIG. 1. **X-ray features of bone healing in WT and *IRS-1*$^{-/-}$ mice.** *A*, the fracture model used in this study. After exposing the right tibiae of 8-week-old mice, a transverse osteotomy was performed at the midshaft with a bone saw. The bone marrow cavity was then stabilized with an intramedullary nail. *B*, time course of the fracture healing in representative WT and *IRS-1*$^{-/-}$ mice. *C*, x-ray features of the fracture sites of all WT mice (n = 15) and *IRS-1*$^{-/-}$ mice (n = 15) at 3 weeks after the fracture. Bone union was completed in all 15 WT mice, whereas in *IRS-1*$^{-/-}$ mice, 12 out of 15 showed non-union (the *12 panels at left*).

IRS-3, and IRS-4 which is expressed in the thymus, brain, and kidney. We reported previously that IRS-1 and IRS-2 are expressed in bone (19, 20). Our further studies on bone metabolism of mice lacking the *IRS-1* gene (*IRS-1*$^{-/-}$ mice) or the *IRS-2* gene (*IRS-2*$^{-/-}$ mice) revealed that IRS-1 is important for maintaining bone turnover (19), whereas IRS-2 is important for maintaining predominance of anabolic function over catabolic function of osteoblasts (20). Regarding the role of these molecules on bone growth, IRS-1, but not IRS-2, seems to play an important role in the growth plate function, because *IRS-1*$^{-/-}$ mice were about 20–30% shorter in limbs and trunk, whereas *IRS-2*$^{-/-}$ mice were normal in size as compared with wild-type (WT) littermates (19–22). These data raise an interesting possibility that IRS-1 may be essential for endochondral ossification. To assess this possibility, the present study investigated the role of IRS-1 in bone healing and its mechanism by an *in vivo* fracture model and an *in vitro* culture system.

EXPERIMENTAL PROCEDURES

Animals—Mice in a C57BL6/CBA hybrid background were generated and maintained as reported previously (21). WT and *IRS-1*$^{-/-}$ male littermates generated from the intercross between heterozygous *IRS-1*$^{+/-}$ mice were compared. All experiments were performed according to the protocol approved by the Animal Care and Use Committee of the University of Tokyo.

Fracture Model—Twenty five male mice at 8 weeks of age were used in each group. Under general anesthesia with pentobarbiturate (0.5 mg/10 g body weight, Sigma), the bilateral hind limbs were shaved and sterilized. A 15-mm incision was made longitudinally over the right leg, and a blunt dissection of the muscle was made to expose the tibia. The middle point of the tibia was marked with a surgical marker, and a transverse osteotomy was performed using a bone saw (Volvere GX, NSK Nakanishi Inc., Tochigi, Japan). The fracture was repositioned, and then the full-length of the bone marrow cavity was internally stabilized with an intramedullary nail using the inner pin of a spinal needle of 22- or 23-gauge diameter depending on the size of the cavity. After irrigation with saline, the skin was sutured. The left tibia (unfractured side) was sham-operated and an intramedullary nail of the same size as the control was inserted. No external fixation was used, and the animals were allowed unrestricted activity as well as diet and water *ad libitum*. For histological analyses, animals were killed at 1 (n = 4/group), 3 (n = 3/group), and 6 weeks (n = 3/group) after the operation by diethyl ether, and bilateral tibiae were excised. After extracting the intramedullary nail gently so as not to injure the fracture site, the soft tissue surrounding the tibiae, except for the soft callus around the fracture site, was removed.

Radiological Analysis—X-ray pictures of the right tibiae of WT and *IRS-1*$^{-/-}$ mice (n = 15 each) were taken at 0 (immediately after the operation), 1–3, 6, and 10 weeks after the operation under general anesthesia using a soft x-ray apparatus (CMB-2; Softex Co., Tokyo, Japan). To determine whether there was bone union, bony bridging on radiographs was evaluated by individuals who were blinded with regard to the genotype of mice.

Measurement of Callus Area and Bone Mineral Content (BMC)—Area and BMC of the entire bilateral tibia were measured by a single energy x-ray absorptiometry utilizing a bone mineral analyzer for small animals (PIXIMUS, Lunar Co., Ltd., WI) at 0 (immediately after the operation), 1–4, and 6 weeks after the operation. A preliminary experiment revealed that the intramedullary nail did not affect the BMC value. The gain of area and the % gain of BMC during observation periods as compared with those at time 0 were calculated for both fractured and unfractured sides, and the differences were compared between WT and *IRS-1*$^{-/-}$.

Histological Analysis—Specimens of the harvested tibiae were fixed with 4% paraformaldehyde in 0.1 mol/liter phosphate buffer, pH 7.4, at 4 °C overnight. After decalcification with 4.13% EDTA at 4 °C for 14 days, the tibiae were dehydrated with an increasing concentration of ethanol, embedded in paraffin, and cut into 4-μm-thick sections. The sections were stained with hematoxylin-eosin (HE) or toluidine blue.

Immunohistochemistry—Immunohistochemical localizations of IRS-1, IRS-2, type X collagen, and proliferating cell nuclear antigen (PCNA) were examined in 4-μm dewaxed paraffin sections. After dehydration, the sections were treated with 0.3% hydrogen peroxide in phosphate-buffered saline (PBS) for 30 min at room temperature. After blocking by PBS containing 1% bovine serum albumin (Sigma) for 1 h at room temperature, the sections were incubated in polyclonal rabbit antibody against IRS-1, IRS-2, or type X collagen (Santa Cruz Biotechnology) or monoclonal mouse antibody against PCNA (PC10, Sigma) (23), at a dilution of 1:100 for 24 h at 4 °C. As negative controls, we used non-immune rabbit IgG and mouse IgG of the same dilution instead of the primary antibodies. Then the sections were rinsed in PBS and incubated with the horseradish peroxidase-conjugated goat antibody against rabbit IgG (Dakopatts, Glostrup, Denmark) for immunohistochemistry of IRS-1, IRS-2, and type X collagen, and with the horseradish peroxidase-conjugated goat antibody against mouse IgG (EY Laboratories, Inc., San Mateo, CA) for that of PCNA, respectively, for 1 h at room temperature. After washing with PBS, the sections were immersed in a diaminobenzidine solution for 10 min at room temperature to visualize immunoreactivity. Terminal transferase dUTP nick-end labeling (TUNEL) staining was performed using an Apoptosis *in Situ* Detection kit (Wako Pure Chemical Co., Ltd., Osaka, Japan) according to the manufacturer's instructions.

Generation of Adenoviruses and Gene Transfer—The recombinant adenovirus vector carrying human *IRS-1* gene engineered to express hemagglutinin tag at its N terminus was constructed using an Adenovirus Expression Vector kit (Takara Shuzo Co., Ltd., Shiga, Japan) following the manufacturer's protocol. The adenovirus vector carrying β-galactosidase gene (AxLacZ) was kindly provided by Dr. I. Saito (University of Tokyo). Two days after the operation, a 1×10^{12} plaque-forming units suspension of AxIRS-1 or AxLacZ was injected into the fracture site of *IRS-1*$^{-/-}$ mice as described previously (24, 25). The same dose of AxLacZ was also injected to WT mice as a positive control. Animals were sacrificed at 1 week (n = 3/group) and 3 weeks (n = 3/group) after the injection. To confirm the infection efficiency, expression of *lacZ* was examined by histochemical staining by X-gal staining

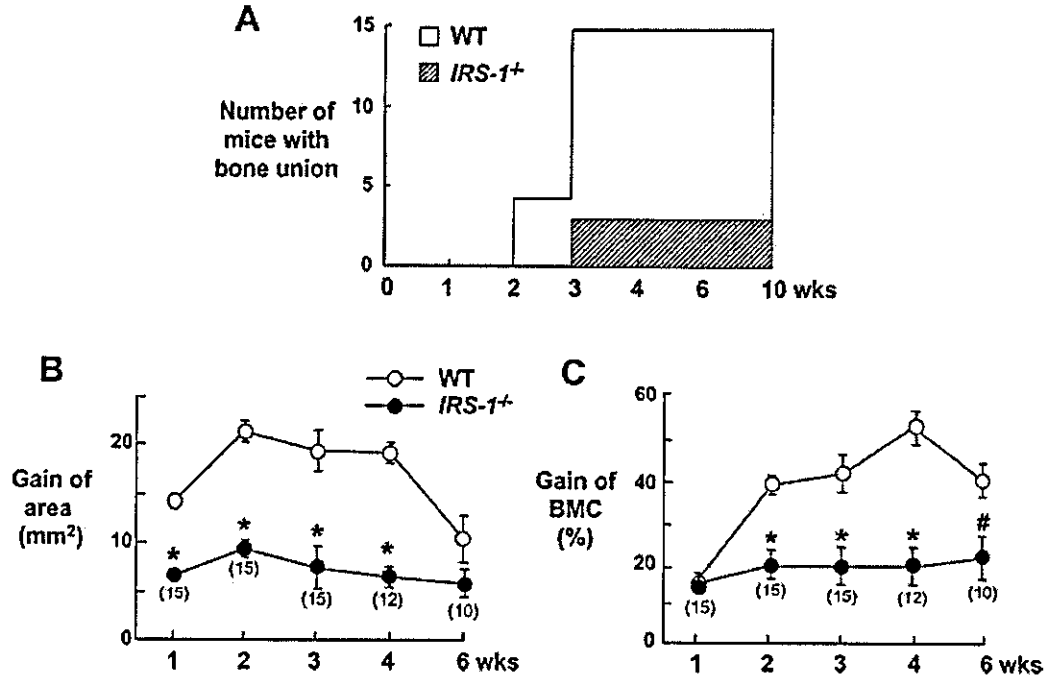

FIG. 2. **Time course of the number of mice with bone union (*A*), the gain of area (*B*), and the % gain of BMC (*C*) at the fracture sites of WT and *IRS-1*$^{-/-}$ mice.** To determine the bone union, the bony bridging at the fracture site on x-rays was judged by individuals blinded with regard to the genotype. The gain of area and the % gain of BMC during observation periods as compared with those at time 0 were calculated for the entire tibiae of fractured and unfractured sides, and the differences were compared between WT and *IRS-1*$^{-/-}$ callus. Because the fracture site became too displaced to measure these parameters correctly at the later stage in *IRS-1*$^{-/-}$ mice, the number of mice was decreased as shown in *parentheses*. Data in *B* and *C* are expressed as the mean (*symbols*) ± S.E. (*error bars*) for 15 WT mice, and the number shown in *parentheses* for *IRS-1*$^{-/-}$ mice. #, $p < 0.05$; *, $p < 0.01$ *versus* WT.

buffer (1 mg/ml X-gal, 5 mM potassium ferrocyanide, and 5 mM potassium ferricyanide) (Wako).

Isolation and Culture of Mouse Growth Plate Chondrocytes—Chondrocytes were isolated from epiphyseal growth plates of WT and *IRS-1*$^{-/-}$ mice at 3.5 weeks of age. Mice were sacrificed, and tibiae were harvested and cleaned of perichondrium in an aseptic manner. Tibiae were pretreated with 0.3% collagenase in serum-free Dulbecco's modified Eagle's medium (DMEM; Sigma) at 37 °C for 30 min to remove residual tissue. By washing the tibiae with PBS, all soft tissues were detached. Growth plates were dissected microscopically by inserting a 26-gauge needle. Subsequently, tibiae were digested with 0.3% collagenase in serum-free DMEM at 37 °C for 5 h, and matrix debris was removed by filtering through a 70-μm cell strainer (BD Biosciences). Chondrocytes were pelleted by centrifugation and washed twice with PBS. Cells were plated in 6-multiwell dishes at a density of 5,000 cells/cm^2 and grown to confluence in DMEM containing 10% FBS and antibiotics in a humidified CO_2 incubator.

X-gal Staining of Chondrocytes Isolated from Transgenic Mice with Type I Collagen Promoter or Type II Collagen Promoter Driving the lacZ Gene—To confirm the purity of chondrocytes isolated by the method above, transgenic mice expressing osteoblast- or chondrocyte-specific marker gene construct (the 2.3-kb fragment of the α1(I) collagen gene promoter or the 1.0-kb fragment of α1(II) collagen promoter and 0.6-kb enhancer) linked to the *Escherichia coli lacZ* gene were used (26, 27). Expression of *lacZ* was examined by histochemical staining with X-gal. Cells were isolated from the growth plates of transgenic mice by the method above and were cultured for 2 days. They were rinsed in PBS twice and fixed with 0.25% glutaraldehyde in PBS on ice for 10 min. After fixed samples were washed in PBS, staining was carried out by the X-gal staining buffer described above at 37 °C overnight.

Western Blot Analysis—To examine the IRS-1 and IRS-2 protein levels, chondrocytes isolated from WT and *IRS-1*$^{-/-}$ growth plates described above were plated in 6-multiwell plates at a density of 10^5 cells/well and incubated in DMEM containing 10% FBS for 24 h. For comparison, we also examined the protein levels in primary osteoblasts that were isolated from neonatal mouse calvariae and cultured in α-minimum Eagle's medium containing 10% FBS as described previously (28). To investigate the signaling pathways through phosphatidylinositol 3-kinase (PI3K)/Akt and mitogen-activated protein kinases (MAPKs), primary chondrocytes were pre-incubated in DMEM containing 10% FBS for 24 h, and treated with IGF-I (10 nM) in the presence and absence of LY294002 (10 μM), PD98059 (10 μM), and SB203580 (10 μM) (all from Calbiochem-Novabiochem) for 30 min. Cells were lysed with TNE buffer (10 mM Tris-HCl, 150 mM NaCl, 1% Nonidet P-40, 1 mM EDTA, 10 mM NaF, 2 mM Na_3VO_4, 1 mM aminoethylbenzenesulfonyl fluoride, and 10 μg/ml aprotinin), and the protein concentration in the cell lysate was measured using a Protein Assay Kit II (Bio-Rad). Equivalent amounts (20 μg) of cell lysates were electrophoresed by 8% SDS-PAGE and transferred to nitrocellulose membrane. After blocking with 5% bovine serum albumin, the membrane was incubated with polyclonal rabbit antibodies against IRS-1 and IRS-2 as described above, Akt, phospho-Akt, extracellular signal-regulated kinase (ERK), phospho-ERK, p38, phospho-p38 MAPK (all from Cell Signaling Technology, Inc. Beverly, MA) and against actin (Sigma). Immunoreactive bands were visualized using the ECL chemiluminescence reaction (Amersham Biosciences) following the manufacturer's instructions. Signals were quantified by densitometry (Bio-Rad).

DNA Synthesis and Proliferation Assays—DNA synthesis and proliferation of isolated chondrocytes were determined by the [^{3}H]thymidine (TdR) uptake and the growth curve, respectively. For the former assay, primary chondrocytes from WT or *IRS-1*$^{-/-}$ mice were inoculated at a density of 5×10^4 cells/well in a 24-multiwell plate and cultured to confluency in DMEM, 10% FBS for 2 days. Serum was withheld for 12 h before adding the experimental medium with or without IGF-I (10 nM), LY294002 (1, 3, and 10 μM), PD98059 (1, 3, and 10 μM), and SB203580 (1, 3, and 10 μM). Uptake of [^{3}H]TdR (1 μCi/ml in the medium) added for the final 2 h was measured at 18 h. For the growth curve assay, primary chondrocytes from WT or *IRS-1*$^{-/-}$ mice were inoculated at a density of 10^5 cells/well in 6-multiwell plates in DMEM, 10% FBS and cultured with or without IGF-I (10 nM). The number of cells/well was counted 1, 3, 5, 7, and 9 days after the seeding.

Statistical Analysis—Means of groups were compared by analysis of variance, and significance of differences was determined by post-hoc testing using Bonferroni's method.

RESULTS

Radiological Findings—Fig. 1A shows an x-ray feature of the fracture model that we used in this study. This model was confirmed to show the bone healing process similar to that in

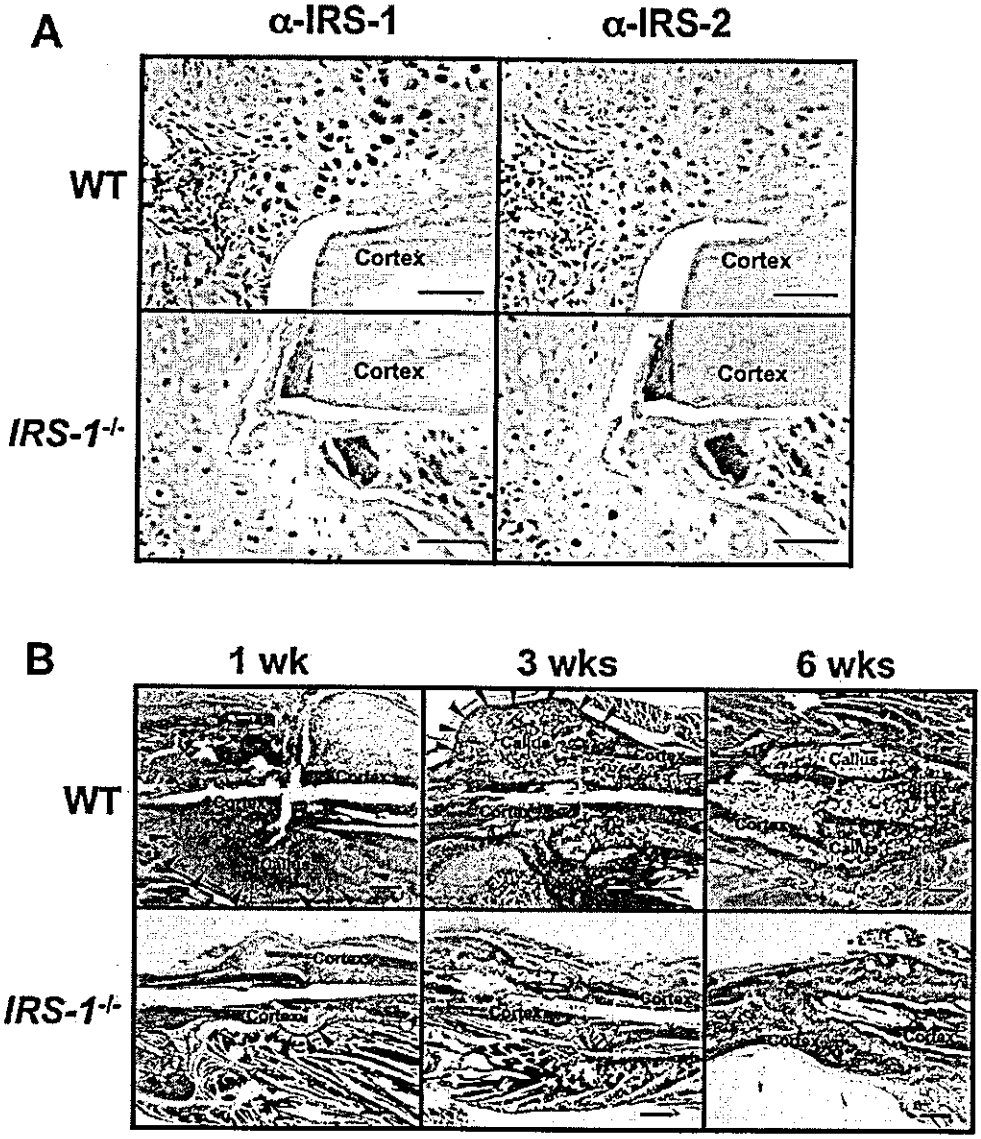

FIG. 3. **Immunolocalization of IRS-1 and IRS-2 (*A*) and time course of histological findings (*B*) at the fracture sites of WT and *IRS-1*$^{-/-}$ mice.** *A*, immunohistochemical stainings with an anti-IRS-1 antibody (*α-IRS-1, left*) and an anti-IRS-2 antibody (*α-IRS-2, right*) were performed on the fracture callus of WT and *IRS-1*$^{-/-}$ mice at 3 weeks. Positive and specific stainings by α-IRS-1 shown in *brown* are seen in fibroblasts and chondrocytes of the WT callus. No immunostaining was observed by the respective non-immune rabbit IgGs as negative controls (data not shown). *Bar*, 100 μm. *B*, 1, 3, and 6 weeks after the fracture, specimens of the harvested tibiae were stained with HE. At 1 week after fracture, the soft callus *outlined* by *arrowheads* is much larger in the WT fracture site than in *IRS-1*$^{-/-}$. At 3 weeks, the WT callus was mineralized as *outlined* by *arrowheads*, which was hardly seen in the *IRS-1*$^{-/-}$ specimen. *Bar*, 1 mm.

humans in a definite temporal sequence by the time course of x-ray examination in WT mice (Fig. 1*B*, *upper panel*). Callus formation could be detected at 1 week, and bony bridging at the fracture site was completed 2 or 3 weeks after the fracture. After the callus size and density reached maximum around 3 weeks, they decreased gradually due to bone remodeling up to 10 weeks. In *IRS-1*$^{-/-}$ mice, however, neither callus formation nor bridging between the fracture stumps was seen at the early stage, and the fracture site became atrophic without bone union at 10 weeks. Fig. 1*C* shows x-ray features of the fracture site of all 15 mice in each of WT and *IRS-1*$^{-/-}$ groups at 3 weeks after fracture. In WT mice, bone union with substantial hard callus formation was observed in all 15 animals. In *IRS-1*$^{-/-}$ mice, however, fracture healing was extremely impaired, and 12 out of 15 mice showed no bone union (the *12 panels at left*). Although bone union was seen in 3 *IRS-1*$^{-/-}$ mice (the *3 panels at right*), the callus looked much smaller and fainter than that of WT mice.

The time course of the number of animals with fracture union determined by bony bridging on x-ray revealed that 4 WT mice achieved bone union at 2 weeks after the operation, and all 15 mice did so at 3 weeks. However, only 3 *IRS-1*$^{-/-}$ mice showed bone union at 3 weeks, but the other 12 animals remained in a non-union state even at 10 weeks (Fig. 2*A*).

Callus Area and BMC—To quantify the callus formation, differences in the gain of area and the % gain of BMC between the fractured and unfractured tibiae were measured by a bone densitometer (Fig. 2, *B* and *C*). Significant differences between WT and *IRS-1*$^{-/-}$ mice were seen from 1 to 4 weeks in the callus area, and from 2 weeks to the end in the BMC. In WT mice, both parameters were increased at the early stage of healing due to the acceleration of the modeling

process and decreased thereafter due to remodeling. In *IRS-1*$^{-/-}$ mice, these parameters remained at low levels throughout the observation period. At the later stage in the *IRS-1*$^{-/-}$ mice, the fracture site became displaced due to non-union, and at 10 weeks more than half the *IRS-1*$^{-/-}$ mice showed severe displacement which was beyond evaluation. To exclude the possibility of other parts of tibiae outside the fracture site affecting BMC, BMC at the bilateral femurs and distal third tibiae was measured at 3 and 6 weeks. Because there were no differences between the fractured and unfractured sides (data not shown), the BMC decrease in *IRS-1*$^{-/-}$ mice was caused by the decrease in that of the callus itself.

Histological Findings—To assess the involvement of IRS-1 and IRS-2 in bone healing, we examined the localizations of these proteins at the fracture site in WT and *IRS-1*$^{-/-}$ mice at 3 weeks after fracture (Fig. 3*A*). Immunohistochemical analysis of WT callus revealed that IRS-1 was localized at various cells including chondrocytes and fibroblasts, although IRS-2 immunoactivity was very faint. In *IRS-1*$^{-/-}$ mice, both IRS-1 and IRS-2 proteins were barely detectable at the fracture site, suggesting that there was no compensatory up-regulation of IRS-2 by IRS-1 deficiency.

Fig. 3*B* shows the temporal comparison of histology between WT and *IRS-1*$^{-/-}$ fracture sites. At 1 week after fracture, tissue reaction was seen in the large areas around the fracture gap in WT mice, whereas in *IRS-1*$^{-/-}$ mice it was markedly decreased, resulting in the reduced size of soft callus. At 3 weeks, mineralized and hard callus due to endochondral ossification was abundantly observed in WT mice, whereas fibrous tissue remained at the fracture gap in *IRS-1*$^{-/-}$ mice. At 6 weeks, bony union after the remodeling was completed in WT mice. However, in *IRS-1*$^{-/-}$ mice, fibrous tissue still remained in the fracture gap, indicating a state of non-union. Thus, the impairment of fracture healing in *IRS-1*$^{-/-}$ mice was seen from the early stage of fracture healing, at which time the required amount of soft callus must be formed.

To learn the cellular and molecular mechanisms of impaired bone healing at the early stage due to IRS-1 deficiency, we performed more detailed histological analyses of the fracture callus at 1 week (Fig. 4). Although the size of soft callus was much smaller in *IRS-1*$^{-/-}$ mice than in WT mice, the chondrocyte differentiation in this small cartilage of *IRS-1*$^{-/-}$ mice was more advanced than that of WT mice as shown by the toluidine blue staining (Fig. 4, *A* and *B*). Type X collagen, a marker for hypertrophic chondrocytes, was much more prevalent in *IRS-1*$^{-/-}$ cartilage than in WT cartilage (Fig. 4, *C* and *D*). We further investigated the proliferation and apoptosis of chondrocytes by PCNA and TUNEL stainings, respectively. PCNA-positive proliferative cells were found massively at the WT callus, although they were faint and scant in the *IRS-1*$^{-/-}$ callus (Fig. 4, *E* and *F*). In contrast, TUNEL-positive apoptotic cells were hardly visible in WT, whereas they were abundant in hypertrophic chondrocytes of *IRS-1*$^{-/-}$ (Fig. 4, *G* and *H*). These findings indicate that the suppression of callus formation in the *IRS-1*$^{-/-}$ fracture site was associated with a decrease in chondrocyte proliferation and increases in hypertrophic differentiation and apoptosis.

Restoration by Reintroduction of IRS-1 in the IRS-1$^{-/-}$ *Fracture*—To confirm that the impairment in fracture healing was due simply to the IRS-1 deficiency in these mice, we injected an adenovirus vector carrying *IRS-1* gene (AxIRS1) or *lacZ* (AxLacZ) to the fracture site 2 days after the fracture. The transgene expression was confirmed by the X-gal staining in and around the AxLacZ-injected fracture sites, which was positively observed intracellularly in various differentiation stages

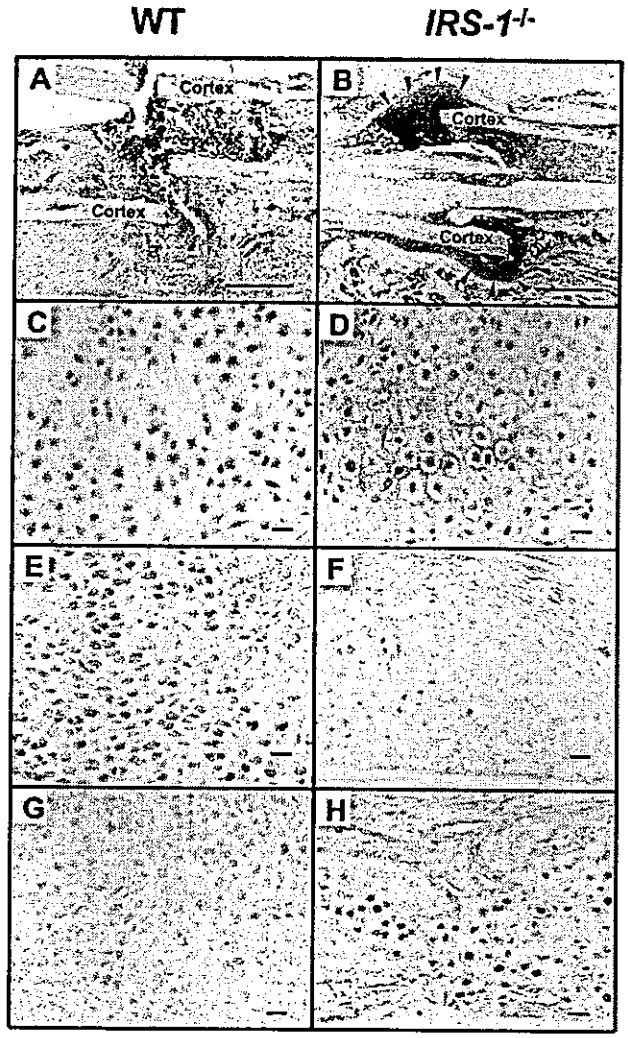

FIG. 4. **Histological and immunohistochemical findings of the soft callus of WT (*A*, *C*, *E*, and *G*) and *IRS-1*$^{-/-}$ mice (*B*, *D*, *F*, and *H*) 1 week after the fracture; toluidine blue (*A* and *B*), type X collagen (*C* and *D*), PCNA (*E* and *F*), and TUNEL (*G* and *H*) stainings.** The 4-μm-thick sections prepared as described for the HE staining were used for the toluidine blue staining. In the WT specimen, the entire fibrous tissue below the fracture site, which is hardly stained with toluidine blue, is the soft callus, whereas in the *IRS-1*$^{-/-}$ specimen, the soft callus *outlined* by *arrowheads* was much smaller but more positively stained (*A* and *B*). Immunohistochemical stainings for type X collagen and TUNEL were examined in 4-μm dewaxed paraffin sections as described under "Experimental Procedures." Both type X collagen-expressing hypertrophic chondrocytes (*C* and *D*) and TUNEL-positive apoptotic cells (*G* and *H*) were more prevalent in the *IRS-1*$^{-/-}$ callus than in WT. On the contrary, PCNA-positive proliferative cells were rarely seen in the *IRS-1*$^{-/-}$ callus (*E* and *F*). No immunostaining was observed by the respective non-immune IgGs as negative controls (data not shown). *Bar*, 1 mm (*A* and *B*) and 10 μm (*C–H*).

of mesenchymal cells (data not shown). AxIRS1 reintroduction to the *IRS-1*$^{-/-}$ fractured site restored the callus area at 1 and 3 weeks, and the callus BMC at 3 weeks after the injection (Fig. 5*A*). Although the restorations did not fully reach the levels of the WT callus injected with AxLacZ, AxIRS1 produced a substantial callus at 1 week (Fig. 5*B*), and all 3 *IRS-1*$^{-/-}$ mice injected with AxIRS-1 showed bony union at 3 weeks, whereas all those injected with AxLacZ remained in a non-union state. It was therefore confirmed that the IRS-1 deficiency *in situ* caused the impaired fracture healing.

Analyses of Cultured Primary Chondrocytes—To clarify fur-

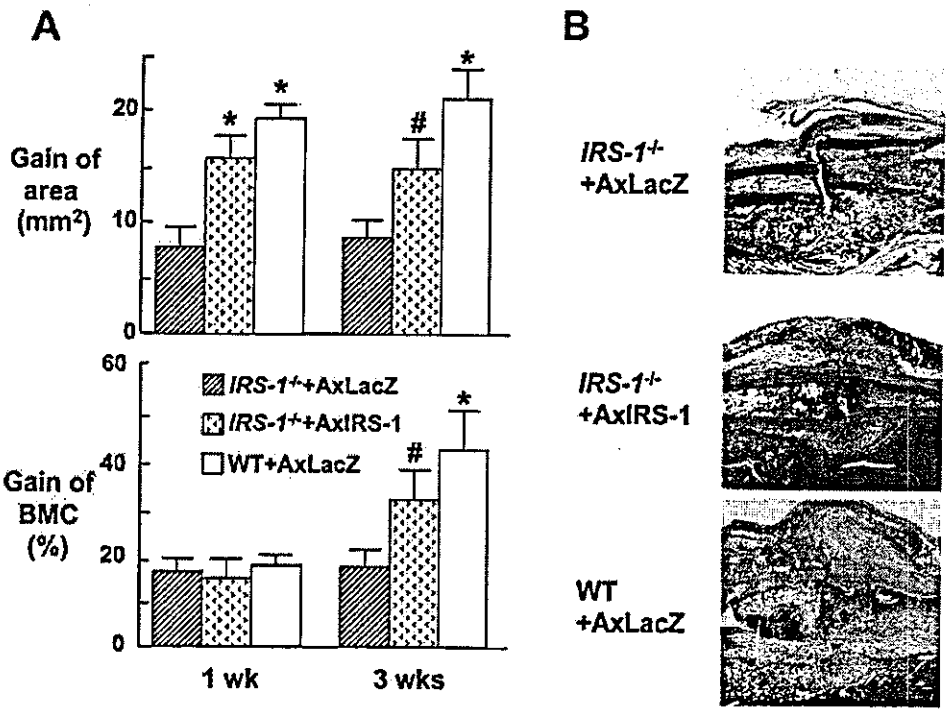

FIG. 5. **Restoration of callus formation by reintroduction of IRS-1 in the *IRS-1*$^{-/-}$ fracture using an adenovirus vector carrying *IRS-1* gene (AxIRS1) or *lacZ* (AxLacZ).** *A*, the gain of area (*upper panel*) and the % gain of BMC (*lower panel*) of the callus in AxLacZ- or AxIRS1-injected *IRS-1*$^{-/-}$ mice and AxLacZ-injected WT mice. AxIRS-1 or AxLacZ was injected into the fracture site of *IRS-1*$^{-/-}$ or WT mice 2 days after the fracture, and animals were sacrificed at 1 week and 3 weeks after the injection. The parameters during the observation periods as compared with those at time 0 were calculated for the entire tibiae of fractured and unfractured sides, and the differences were compared between WT and *IRS-1*$^{-/-}$. Data are expressed as the mean (*bars*) ± S.E. (*error bars*) for 3 mice/group. #, $p < 0.05$; *, $p < 0.01$ *versus* *IRS-1*$^{-/-}$+AxLacZ. *B*, HE staining of the callus 1 week after the injection.

ther the cellular mechanisms underlying these abnormalities, we used our original method to isolate chondrocytes from the growth plate. We first confirmed the purity of the growth plate chondrocytes by the X-gal staining of cultured chondrocytes isolated by this method from the transgenic mice expressing the *lacZ* reporter gene driven by a promoter fragment of type I collagen (*COL1-LacZ*) or type II collagen gene (*COL2-LacZ*) (26, 27). More than 99% of the cells isolated from transgenic mice with the type II collagen promoter were stained X-gal-positive, indicating positive *lacZ* transgene expression, whereas none of the cells from type I collagen promoter-driving transgenic mice exhibited the expression (Fig. 6*A*). These results demonstrate that almost all cells isolated from the growth plate by this method are cells of chondrocyte lineage and are not contaminated by other cells such as osteoblasts or fibroblasts, which express type I collagen.

To confirm the expression patterns of IRS-1 and IRS-2 as shown in Fig. 3*A*, we examined the protein levels in the growth plate chondrocytes by Western blottings using the same antibodies as Fig. 3*A* (Fig. 6*B*). WT chondrocytes, but not *IRS-1*$^{-/-}$ chondrocytes, were shown to express the IRS-1 protein; however, neither WT nor *IRS-1*$^{-/-}$ chondrocytes expressed IRS-2. This was not due to the lack of immunoreactivity of the IRS-2 antibody since IRS-2 protein could be detected in primary osteoblasts, the positive control cells that we studied previously (20).

We then compared DNA synthesis and proliferation of the primary chondrocytes between WT and *IRS-1*$^{-/-}$ by the [^{3}H]TdR uptake (Fig. 6*C*) and the growth curve (Fig. 6*D*), respectively. *IRS-1*$^{-/-}$ chondrocytes showed significantly reduced [^{3}H]TdR uptake as compared with WT chondrocytes in the control culture (Fig. 6*C*). Both IGF-I and insulin significantly stimulated the DNA synthesis of WT chondrocytes but not that of *IRS-1*$^{-/-}$ chondrocytes. On the other hand, the stimulation by FGF-2 was similarly seen in both WT and *IRS-1*$^{-/-}$ chondrocytes, indicating that impaired DNA synthesis in cultured *IRS-1*$^{-/-}$ chondrocytes was specific to IGF-I and insulin. The growth curve for 9 days after the seeding confirmed the impaired mitogenic ability of *IRS-1*$^{-/-}$ chondrocytes (Fig. 6*D*). The number of these chondrocytes was significantly lower than that of WT chondrocytes at 7 days and thereafter in the control cultures, and the difference was enhanced in the presence of IGF-I.

Signal Transduction in Cultured Primary Chondrocytes—To provide some insight into signaling pathways that are affected by the IRS-1 deficiency in chondrocytes, we compared the activation of PI3K/Akt and MAPKs, the main signals lying downstream of IRS-1, between WT and *IRS-1*$^{-/-}$ growth plate chondrocytes (Fig. 7*A*). Western blot analyses of the WT chondrocytes revealed that IGF-I induced phosphorylations of Akt and ERK but not that of p38 MAPK. Specific inhibitors, LY294002, PD98059, and SB203580, were confirmed to inhibit the phosphorylations of Akt, ERK, and p38 MAPK, respectively. In the *IRS-1*$^{-/-}$ chondrocytes, the Akt phosphorylation by IGF-I was reduced as compared with that of WT chondrocytes; however, phosphorylations of ERK and p38 MAPK were similar between WT and *IRS-1*$^{-/-}$ chondrocytes. The decrease in the Akt phosphorylation by the IRS-1 deficiency was confirmed by quantitative analyses using densitometry in independent Western blottings of three separate experiments (Fig. 7*B*). These results indicate that the IRS-1 deficiency led to impairment of the PI3K/Akt pathway but not the MAPK pathways.

To examine further the involvement of these signaling pathways in the mitogenic action of IGF-I on the WT and *IRS-1*$^{-/-}$ chondrocytes, the inhibitors above were added to the chondro-

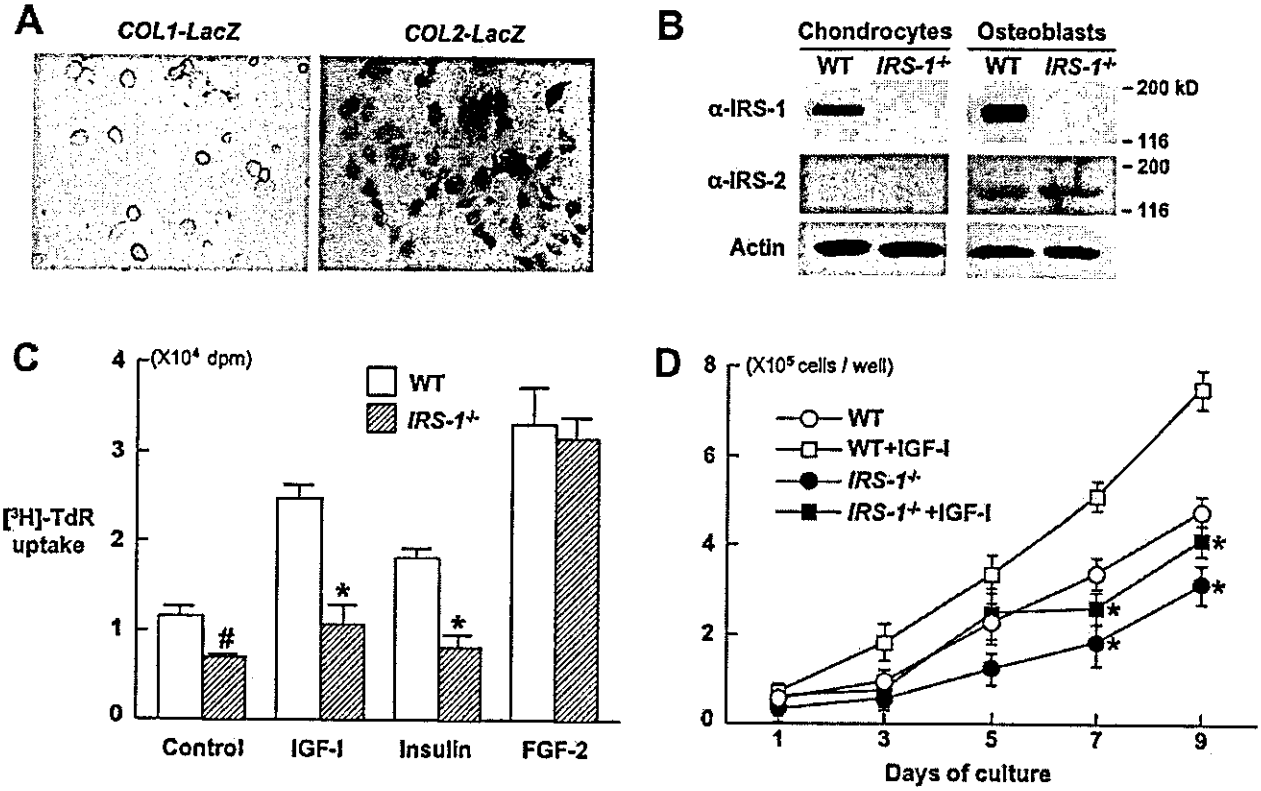

FIG. 6. **Characterization and proliferation of chondrocytes isolated from WT and *IRS-1*$^{-/-}$ growth plates.** *A*, chondrocytes were isolated from epiphyseal growth plates of WT and *IRS-1*$^{-/-}$ mice at 3.5 weeks of age as described under "Experimental Procedures." To confirm the purity of chondrocytes, cells were isolated from the growth plates of transgenic mice expressing the *lacZ* reporter gene driven by the type I collagen promoter gene fragment (*COL1-LacZ*) or the type II collagen promoter gene fragment (*COL2-LacZ*). LacZ activity was visualized as *blue* with X-gal staining. *B*, Western blottings for the IRS-1 and IRS-2 expressions in the growth plate chondrocytes and calvarial osteoblasts derived from WT and *IRS-1*$^{-/-}$ mice. Antibodies for IRS-1 and IRS-2 (α-IRS-1 and α-IRS-2) were the same as those used in the immunohistochemical analyses (Fig. 3*A*). *C*, DNA synthesis determined by [^{3}H]TdR uptake in chondrocytes isolated from WT and *IRS-1*$^{-/-}$ growth plates cultured with and without insulin (100 nM), IGF-I (10 nM), or FGF-2 (10 nM) for 18 h. Data are expressed as the mean (*bars*) ± S.E. (*error bars*) for 8 wells/group. #, $p < 0.05$; *, $p < 0.01$ *versus* WT culture. *D*, cell proliferation determined by growth curves of chondrocytes that were isolated from WT and *IRS-1*$^{-/-}$ growth plates and cultured in the presence and absence of IGF-I. Chondrocytes were inoculated at a density of 10^5 cells/well in 6-multiwell plates, and the number of the cells/well was counted 1, 3, 5, 7, and 9 days after the seeding. Data are expressed as the mean (*symbols*) ± S.E. (*error bars*) for 6 wells/group. *, $p < 0.01$; significant decrease by the IRS-1 deficiency.

cyte cultures (Fig. 7*C*). LY294002, an Akt inhibitor, dose-dependently decreased the stimulation of [^{3}H]TdR uptake by IGF-I in the WT culture; however, in the *IRS-1*$^{-/-}$ culture, the inhibition was not statistically significant ($p > 0.05$). PD98059, an ERK inhibitor, decreased the IGF-I mitogenic effect at the highest concentration of 10 μM both in the WT and *IRS-1*$^{-/-}$ cultures ($p < 0.01$), whereas SB203580, a p38 inhibitor, did not affect it in either culture. Taken together, these results suggest that the mitogenic action of IGF-I is mediated largely by the IRS-1-dependent pathway through the PI3K/Akt activation and partly by IRS-1-independent pathway through the ERK activation.

DISCUSSION

Although IRS-1 and IRS-2 are known to be essential for intracellular signaling of IGF-I/insulin, these two adaptor molecules have distinct biological roles and are differentially expressed in a variety of cells. Regarding glucose homeostasis, IRS-1 plays an important role in the metabolic actions of insulin mainly in skeletal muscle and adipose tissue, whereas IRS-2 does so in the liver (29, 30). For bone metabolism, although both are expressed in osteoblasts, they play distinct roles in the anabolic function of IGF-I and insulin (19, 20). The present study, however, failed to detect the IRS-2 expression in isolated chondrocytes or fracture callus. Our previous studies also revealed that IRS-2 was not expressed in the epiphyseal cartilage (31) and that *IRS-2*$^{-/-}$ mice showed normal epiphyseal cartilage and skeletal growth as opposed to *IRS-1*$^{-/-}$ mice (20). We therefore speculate that IRS-2 is much less important than IRS-1 in bone regeneration through endochondral ossification such as bone healing and skeletal growth. In fact, our preliminary experiment showed no abnormality of bone healing in *IRS-2*$^{-/-}$ mice (data not shown).

Because histological examinations suggested the central role of abnormal chondrocyte functions in the impairment of bone healing by the IRS-1 deficiency, we focused on the chondrocyte culture to study the cellular and molecular mechanisms. For this study, we avoided using the conventional chondrocyte culture system derived from the rib cartilage of neonatal mice (32), because most of the cartilage belongs to the permanent cartilage that does not undergo endochondral ossification but maintains cartilage phenotypes. Instead, we succeeded in isolating chondrocytes from the growth plate with more than 99% purity, as confirmed by the X-gal staining of cultured cells from transgenic mice expressing osteoblast- or chondrocyte-specific marker genes (Fig. 6*A*). Our preliminary study has confirmed that the growth plate chondrocytes showed much higher ability of proliferation than the rib chondrocytes. However, neither hypertrophic differentiation nor apoptosis could be clearly observed even after long term culture of the growth plate chondrocytes. Hence, although we believe that the present chon-

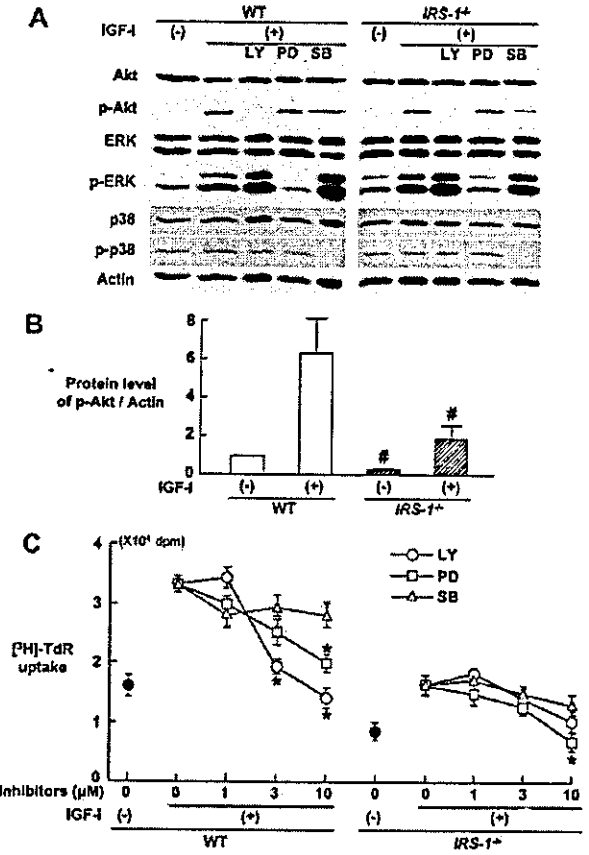

FIG. 7. **Intracellular signaling in the WT and *IRS-1*$^{-/-}$ growth plate chondrocytes.** *A*, effects of IGF-1 and specific inhibitors on phosphorylations of Akt, ERK, and p38 MAPK in cultured chondrocytes. The chondrocytes were isolated as above and cultured with and without IGF-I (10 nM) in the presence and absence of an Akt inhibitor LY294002 (*LY*, 10 μM), an ERK inhibitor PD98059 (*PD*, 10 μM), and p38 MAPK inhibitor SB203580 (*SB*, 10 μM) for 30 min. Western blottings were performed as described under "Experimental Procedures." *B*, quantitative analysis of phospho-Akt (*p-Akt*) levels determined by three independent Western blottings using samples from separate experiments including that above (*A*). The *ordinate axis* shows the intensity of the p-Akt band normalized to that of β-actin measured by densitometry. The graph indicates means (*bars*) ± S.E. (*error bars*) of the ratio values as compared with that of WT control group in three independent experiments. #, $p < 0.05$; significant decrease by the IRS-1 deficiency. *C*, effects of specific inhibitors on the mitogenic action of IGF-I in cultured primary chondrocytes. The primary chondrocytes were cultured with and without IGF-I (10 nM), LY294002 (1, 3, and 10 μM), PD98059 (1, 3, and 10 μM), and SB203580 (1, 3, and 10 μM). After 18 h of culture, DNA synthesis was determined by [³H]TdR uptake. Data are expressed as means (*symbols*) ± S.E. (*error bars*) for 8 wells/group. *, $p < 0.01$, significant inhibition by LY294002, PD98059, or SB203580.

drocyte culture system is more suitable for studies on the proliferation of chondrocytes than the conventional culture system, a culture system of primary cells isolated directly from the fracture callus will be much more appropriate to study the mechanisms underlying impaired fracture healing in *IRS-1*$^{-/-}$ mice. In fact, we initially tried to use these callus-derived cells for the culture; however, the callus was composed of cells of heterogeneous kinds at various differentiation stages so that the data were too inconsistent to compare among animals.

The *IRS-1*$^{-/-}$ callus exhibited not only a decrease in proliferation of chondrocytes but also increases in hypertrophic differentiation and apoptosis (Fig. 4). This is compatible with our histological findings of the *IRS-1*$^{-/-}$ growth plate, which showed a decrease in the height of the proliferating zone and an early closure of the growth plate, resulting in a reduced longitudinal bone growth (31). Although the mechanism of the decrease in chondrocyte proliferation by the IRS-1 deficiency was shown by the growth plate chondrocyte cultures, that of the increase in differentiation or apoptosis remains unclarified. Because chondrocytes are known to start hypertrophic differentiation in synchrony with the cessation of proliferation, the acceleration of chondrocyte differentiation and the subsequent apoptosis seen in the *IRS-1*$^{-/-}$ fracture callus and growth plate might be secondary to the impairment of proliferation. However, there are several reports (33–38) showing that IRS-1 directly inhibits differentiation and apoptosis in hemopoietic and neuronal cells and that these inhibitions are partly associated with an increase in the cell size. Although the present *in vivo* and *in vitro* studies did not find the change of cell size of chondrocytes by the IRS-1 deficiency, the possible involvement of direct action of IRS-1 signaling in differentiation and apoptosis cannot be denied. As mentioned above, studies on these aspects using a culture system of other primary chondrocytes in which both hypertrophy and apoptosis can be properly assessed will be the next task for investigation.

The decreased [³H]TdR uptake in *IRS-1*$^{-/-}$ chondrocytes was seen not only in the stimulated culture by IGF-I or insulin but also in the control culture (Fig. 6*C*). This may be due to the blockage of signalings of endogenous IGF-I as an autocrine/paracrine factor in the culture. The concentrations of IGF-I in the culture medium were 0.79 ± 0.20 and 0.66 ± 0.15 nM (mean ± S.E.) in the control WT and *IRS-1*$^{-/-}$ cultures, respectively. In addition, our previous study has shown that serum IGF-I levels were similar between WT and *IRS-1*$^{-/-}$ mice, suggesting the absence of systemic compensation for impaired IGF-I activity (19). Hence, the impaired fracture healing in *IRS-1*$^{-/-}$ mice might be due to the deficit of anabolic signaling of endogenous IGF-I produced by chondrocytes acting as an autocrine/paracrine factor. Impairment of *IRS-1*$^{-/-}$ fracture healing might partly be caused by systemic hormones, of which actions are mediated by IGF-I. Growth hormone is a well known stimulus of IGF-I production in a variety of tissues, including bone, and exerts its effects on bone mainly through IGF-I mediation (39). Parathyroid hormone also increases IGF-I production, and decreases of IGF-I signaling can block selective anabolic actions of parathyroid hormone on bone (40, 41). Similarly, other hormones with effects on bone such as cortisol (42), thyroid hormone (43), estrogen (44), and androgens (45) alter IGF-I levels in bone in a manner consistent with IGF-I playing a role in the actions of these hormones on bone.

It is noteworthy that skeletal phenotypes of IGF-I receptor (IGF-IR) and IGF-I-deficient mice are rather different from that of *IRS-1*$^{-/-}$ mice. First, they exhibit more severe growth retardation than do *IRS-1*$^{-/-}$ mice (5, 6, 46). More important, the closure of the growth plate is delayed in *IGF-I*$^{-/-}$ mice (5, 6), whereas it is accelerated in *IRS-1*$^{-/-}$ mice (31). These discrepancies might be due to the 66-kDa Src homology collagen (SHC), another adaptor protein phosphorylated by the IGF-IR activation, which is reported to be expressed in chondrocytes and osteoblasts (47, 48). SHC is known to associate with growth factor receptor-bound protein 2, p21 Ras, and a serine/threonine kinase cascade leading to the activation of ERK in chondrocytes (47, 49, 50). Our Western blotting data that IGF-I induced phosphorylations of both Akt and ERK, whereas IRS-I deficiency decreased only the Akt phosphorylation in Fig. 7*A*, support the existence of SHC/ERK pathway in chondrocytes. Inhibition of this pathway by PD98059 may cause the suppression of the IGF-I mitogenic effect in both WT and *IRS-1*$^{-/-}$

cultures (Fig. 7*C*). Most interesting, IGF-I induced the Akt phosphorylation not only in WT but also in *IRS-1*$^{-/-}$ chondrocytes (Fig. 7, *A* and *B*), suggesting the involvement of SHC/Ark pathway in a downstream signaling of IGF-IR activation. This pathway, however, seems functionally less important than IRS-1/Akt and SHC/ERK pathways, because the inhibition by LY294002 was not statistically significant in the *IRS-1*$^{-/-}$ culture (Fig. 7*C*). It is also important that the SHC signaling positively regulates apoptosis (51). A decrease in the apoptotic pathway through SHC may cause the delay of the growth plate closure in the *IGF-I*$^{-/-}$ mice, whereas the compensatory up-regulation of the SHC signaling might lead to accelerated apoptosis of chondrocytes at the fracture callus and the growth plate in *IRS-1*$^{-/-}$ mice. Studies on the skeletal phenotype of the SHC-deficient mice will lead to elucidation of the differential regulation of bone regeneration by IRS-1 and SHC signalings.

We hereby conclude that the IRS-1 deficiency impairs bone healing at least partly by inhibiting the chondrocyte proliferation through the PI3K/Akt pathway, and we propose that IRS-1 can be a target molecule for bone regenerative medicine. There are several recent reports (52, 53) that used bone fracture models to identify *in vivo* signalings, such as tumor necrosis factor-α and cyclooxygenase-2, which play essential roles in the osteogenic process. Because IRS-1 is an intracellular protein, we are planning to use the gene transfer into precursor cells by using conventional natural viruses or nonviral vectors that we are now developing (54). In the present study, the *in vivo* fracture system and the *in vitro* chondrocyte culture system were applied for the first time in combination to investigate the role of a certain molecule in knockout mice. This approach seems useful for elucidating a network of molecules implicated in bone regeneration.

REFERENCES

1. Bolander, M. E. (1992) *Proc. Soc. Exp. Biol. Med.* **200**, 165–170
2. Kawaguchi, H., Kurokawa, T., Hanada, K., Hiyama, Y., Tamura, M., Ogata, E., and Matsumoto, T. (1994) *Endocrinology* **135**, 774–781
3. Canalis, E. (1993) *Bone (NY)* **14**, 273–276
4. Laron, Z. (2001) *Mol. Pathol.* **54**, 311–316
5. Liu, J. P., Baker, J., Perkins, A. S., Robertson, E. J., and Efstratiadis, A. (1993) *Cell* **75**, 59–72
6. Powell-Braxton, L., Hollingshead, L. P., Warburton, C., Dowd, M., Pitts-Meek, S., Dalton, D., Gillett, N., and Stewart, T. A. (1993) *Genes Dev.* **7**, 2609–2617
7. Laron, Z., Klinger, B., and Silbergeld, A. (1999) *J. Bone Miner. Res.* **14**, 156–157
8. Trippel, S. B. (1998) *Clin. Orthop. Relat. Res.* **355**, S301–S313
9. Schmidmaier, G., Wildemann, B., Heeger, J., Gabelein, T., Flyvbjerg, A., Bail, H. J., and Raschke, M. (2002) *Bone (NY)* **31**, 165–172
10. Thomas, D. M., Hards, D. K., Rogers, S. D., Ng, K. W., and Best, J. D. (1997) *Endocrinol. Metab. Clin North Am.* **4**, 5–17
11. Shukunami, C., Shigeno, C., Atsumi, T., Ishizeki, K., Suzuki, F., and Hiraki, Y. (1996) *J. Cell Biol.* **133**, 457–468
12. Kato, Y., and Gospodarowicz, D. (1984) *J. Cell Physiol.* **120**, 354–363
13. Krakauer, J. C., McKenna, M. J., Rao, D. S., and Whitehouse, F. W. (1997) *Diabetes Care* **20**, 1339–1340
14. Piepkorn, B., Kann, P., Forst, T., Andreas, J., Pfutzner, A., and Beyer, J. (1997) *Horm. Metab. Res.* **29**, 584–591
15. Macey, L. R., Kana, S. M., Jingushi, S., Terek, R. M., Borretos, J., and Bolander, M. E. (1989) *J. Bone Jt. Surg. Am.* **71**, 722–733
16. Loder, R. T. (1988) *Clin. Orthop.* **232**, 210–216
17. Burks, D. J., and White, M. F. (2001) *Diabetes* **50**, Suppl. 1, 140–145
18. Kadowaki, T., Tobe, K., Honda-Yamamoto, R., Tamemoto, H., Kaburagi, Y., Momomura, K., Ueki, K., Takahashi, Y., Yamauchi, T., Akanuma, Y., and Yazaki, Y. (1996) *Endocr. J.* **43**, (suppl.) 33–41
19. Ogata, N., Chikazu, D., Kubota, N., Terauchi, Y., Tobe, K., Azuma, Y., Ohta, T., Kadowaki, T., Nakamura, K., and Kawaguchi, H. (2000) *J. Clin. Invest.* **105**, 935–943
20. Akune, T., Ogata, N., Hoshi, K., Kubota, N., Terauchi, Y., Tobe, K., Azuma, Y., Kadowaki, T., Nakamura, K., and Kawaguchi, H. (2002) *J. Cell Biol.* **159**, 147–156
21. Tamemoto, H., Kadowaki, T., Tobe, K., Yagi, T., Sakura, H., Hayakawa, T., Terauchi, Y., Ueki, K., Kaburagi, Y., Satoh, S., Sekihara, H., Yoshioka, Y., Horikoshi, H., Furuta, Y., Ikawa, Y., Kasuga, M., Yazaki, Y., and Aizawa, S. (1994) *Nature* **372**, 182–186
22. Kubota, N., Tobe, K., Terauchi, Y., Eto, K., Yamauchi, T., Suzuki, R., Tsubamoto, Y., Komeda, K., Nakano, R., Miki, H., Satoh, S., Sekihara, H., Sciacchitano, S., Lesniak, M., Aizawa, S., Nagai, R., Kimura, S., Akanuma, Y., Taylor, S. I., and Kadowaki, T. (2000) *Diabetes* **49**, 1880–1889
23. Smink, J. J., Gresnigt, M. G., Hamers, N., Koedam, J. A., Berger, R., and Van Buul-Offers, S. C. (2003) *J. Endocrinol.* **177**, 381–388
24. van Griensven, M., Lobenhoffer, P., Barke, A., Tschernig, T., Lindenmaier, W., Krettek, C., and Gerich, T. G. (2002) *Lab. Anim.* **36**, 455–461
25. Uusitalo, H., Hiltunen, A., Ahonen, M., Gao, T. J., Lefebvre, V., Harley, V., Kahari, V. M., and Vuorio, E. (2001) *J. Bone Miner. Res.* **16**, 1837–1845
26. Liu, W., Toyosawa, S., Furuichi, T., Kanatani, N., Yoshida, C., Liu, Y., Himeno, M., Narai, S., Yamaguchi, A., and Komori, T. (2001) *J. Cell Biol.* **155**, 157–166
27. Ueta, C., Iwamoto, M., Kanatani, N., Yoshida, C., Liu, Y., Enomoto-Iwamoto, M., Ohmori, T., Enomoto, H., Nakata, K., Takada, K., Kurisu, K., and Komori, T. (2001) *J. Cell Biol.* **153**, 87–100
28. Shimoaka, T., Ogasawara, T., Yonamine, A., Chikazu, D., Kawano, H., Nakamura, K., Itoh, N., and Kawaguchi, H. (2002) *J. Biol. Chem.* **277**, 7493–7500
29. Bruning, J. C., Winnay, J., Cheatham, B., and Kahn, C. R. (1997) *Mol. Cell. Biol.* **17**, 1513–1521
30. Yamauchi, T., Tobe, K., Tamemoto, H., Ueki, K., Kaburagi, Y., Yamamoto-Honda, R., Takahashi, Y., Yoshizawa, F., Aizawa, S., Akanuma, Y., Sonenberg, N., Yazaki, Y., and Kadowaki, T. (1996) *Mol. Cell. Biol.* **16**, 3074–3084
31. Hoshi, K., Ogata, N., Shimoaka, T., Terauchi, Y., Kadowaki, T., Kenmotsu, S., Chung, U., Ozawa, H., Nakamura, K., and Kawaguchi, H. (2004) *J. Bone Miner. Res.* **19**, 214–223
32. Lefebvre, V., Garofalo, S., Zhou, G., Mesaranta, M., Vuorio, E., and de Crombrugghe, B. (1994) *Matrix Biol.* **14**, 329–335
33. Valentinis, B., and Baserga, R. (2001) *Mol. Pathol.* **54**, 133–137
34. Morrione, A., Navarro, M., Romano, G., Dews, M., Reiss, K., Valentinis, B., Belletti, B., and Baserga, R. (2001) *Oncogene* **20**, 4842–4852
35. Valentinis, B., Navarro, M., Zanocco-Marani, T., Edmonds, P., McCormick, J., Morrione, A., Sacchi, A., Romano, G., Reiss, K., and Baserga, R. (2000) *J. Biol. Chem.* **275**, 25451–25459
36. Peruzzi, F., Prisco, M., Dews, M., Salomoni, P., Grassilli, E., Romano, G., Calabretta, B., and Baserga, R. (1999) *Mol. Cell. Biol.* **19**, 7203–7215
37. Hermanto, U., Zong, C. S., Li, W., and Wang, L. H. (2002) *Mol. Cell. Biol.* **22**, 2345–2365
38. Pende, M., Kozma, S. C., Jaquet, M., Oorschot, V., Burcelin, R., Le Marchand-Brustel, Y., Klumperman, J., Thorens, B., and Thomas, G. (2000) *Nature* **408**, 994–997
39. Ohlsson, C., Bengtsson, B. A., Isaksson, O. G., Andreassen, T. T., and Slootweg, M. C. (1998) *Endocr. Rev.* **19**, 55–79
40. Canalis, E., Centrella, M., Burch, W., and McCarthy, T. L. (1989) *J. Clin. Investig.* **83**, 60–65
41. Miyakoshi, N., Kasukawa, Y., Linkhart, T. A., Baylink, D. J., and Mohan, S. (2001) *Endocrinology* **142**, 4349–4356
42. McCarthy, T. L., Centrella, M., and Canalis, E. (1990) *Endocrinology* **126**, 1569–1575
43. Huang, B. K., Golden, L. A., Tarjan, G., Madison, L. D., and Stern, P. H. (2000) *J. Bone Miner. Res.* **15**, 188–197
44. Ernst, M., and Rodan, G. A. (1991) *Mol. Endocrinol.* **5**, 1081–1089
45. Gori, F., Hofbauer, L. C., Conover, C. A., and Khosla, S. (1999) *Endocrinology* **140**, 5579–5586
46. Araki, E., Lipes, M. A., Patti, M. E., Bruning, J. C., Haag, B., Johnson, R. S., and Kahn, C. R. (1994) *Nature* **372**, 186–190
47. Shakibaei, M., John, T., De Souza, P., Rahmanzadeh, R., and Merker, H. J. (1999) *Biochem. J.* **342**, 615–623
48. Caverzasio, J., Palmer, G., Suzuki, A., and Bonjour, J. P. (1997) *J. Bone Miner. Res.* **12**, 1975–1983
49. Lopaczynski, W. (1999) *Acta Biochim. Pol.* **46**, 51–60
50. Benito, M., Valverde, A. M., and Lorenzo, M. (1996) *Int. J. Biochem. Cell Biol.* **28**, 499–510
51. Migliaccio, E., Giorgio, M., Mele, S., Pelicci, G., Reboldi, P., Pandolfi, P. P., Lanfrancone, L., and Pelicci, P. G. (1999) *Nature* **402**, 309–313
52. Zhang, X., Schwarz, E. M., Young, D. A., Puzas, J. E., Rosier, R. N., and O'Keefe, R. J. (2002) *J. Clin. Investig.* **109**, 1405–1415
53. Gerstenfeld, L. C., Cho, T. J., Kon, T., Aizawa, T., Tsay, A., Fitch, J., Barnes, G. L., Graves, D. T., and Einhorn, T. A. (2003) *J. Bone Miner. Res.* **18**, 1584–1592
54. Itaka, K., Harada, A., Nakamura, K., Kawaguchi, H., and Kataoka, K. (2002) *Biomacromolecules* **3**, 841–845

JOURNAL OF BONE AND MINERAL RESEARCH
Volume 19, Number 7, 2004
Published online on May 24, 2004; doi: 10.1359/JBMR.040513

Osteoclast Differentiation by RANKL Requires NF-κB–Mediated Downregulation of Cyclin-Dependent Kinase 6 (Cdk6)

Toru Ogasawara,[1] Mika Katagiri,[1] Aiichiro Yamamoto,[1] Kazuto Hoshi,[1] Tsuyoshi Takato,[1] Kozo Nakamura,[1] Sakae Tanaka,[1] Hiroto Okayama,[2] and Hiroshi Kawaguchi[1]

ABSTRACT: This study investigated the involvement of cell cycle factors in RANKL-induced osteoclast differentiation. Among the G1 cell cycle factors, Cdk6 was found to be a key molecule in determining the differentiation rate of osteoclasts as a downstream effector of the NF-κB signaling.

Introduction: A temporal arrest in the G1 phase of the cell cycle is a prerequisite for cell differentiation, making it possible that cell cycle factors regulate not only the proliferation but also the differentiation of cells. This study investigated cell cycle factors that critically influence differentiation of the murine monocytic RAW264.7 cells to osteoclasts induced by RANKL.

Materials and Methods: Growth-arrested RAW cells were stimulated with serum in the presence or absence of soluble RANKL (100 ng/ml). Expressions of the G1 cell cycle factors cyclin D1, D2, D3, E, cyclin-dependent kinase (Cdk) 2, 4, 6, and Cdk inhibitors (p18 and p27) were determined by Western blot analysis. Involvement of NF-κB and c-*jun* N-terminal kinase (JNK) pathways was examined by overexpressing dominant negative mutants of the *IκB kinase 2* (IKK^{DN}) gene and *mitogen-activated protein kinase kinase 7* ($MKK7^{DN}$) gene, respectively, using the adenovirus vectors. To determine the direct effect of Cdk6 on osteoclast differentiation, stable clones of RAW cells transfected with *Cdk6* cDNA were established. Osteoclast differentiation was determined by TRACP staining, and cell cycle regulation was determined by BrdU uptake and flow cytometric analysis.

Results and Conclusion: Among the cell cycle factors examined, the Cdk6 level was downregulated by RANKL synchronously with the appearance of multinucleated osteoclasts. Inhibition of the NF-κB pathway by IKK^{DN} overexpression, but not that of the JNK pathway by $MKK7^{DN}$ overexpression, caused the decreases in both Cdk6 downregulation and osteoclastogenesis by RANKL. RAW cells overexpressing Cdk6 resist RANKL-induced osteoclastogenesis; however, cell cycle regulation was not affected by the levels of Cdk6 overexpression, suggesting that the inhibitory effect of Cdk6 on osteoclast differentiation was not exerted through cell cycle regulation. These results indicate that Cdk6 is a critical regulator of RANKL-induced osteoclast differentiation and that its NF-κB–mediated downregulation is essential for efficient osteoclast differentiation.

J Bone Miner Res 2004;19:1128–1136. Published online on May 24, 2004; doi: 10.1359/JBMR.040513

Key words: osteoclast, cyclin, cell cycle, RANKL, bone

INTRODUCTION

OSTEOCLASTS ARE DERIVED from hematopoietic myeloid precursors of monocyte/macrophage lineage under the control of systemic and local factors produced by supporting cells such as osteoblasts and bone marrow stromal cells. Among these factors, RANKL is a TNF-related cytokine that stimulates osteoclast differentiation from hematopoietic precursor cells both in vitro and in vivo.[1–3] Mice lacking in either RANKL or its receptor RANK have defects in osteoclast differentiation that lead to severe osteopetrosis.[4–6] RANK is expressed on the surface of osteoclast progenitor cells and induces intracellular signals, leading to osteoclastogenesis on ligand binding or agonistic anti-RANK antibody stimulation.[6,7] Like other TNF receptor superfamily members, RANK stimulation can induce NF-κB, probably through association with several TNF receptor–associated factors (TRAFs): TRAF2, TRAF5, and TRAF6.[6,8–11] Mice deficient in both p50 and p52 subunits of NF-κB have been found to be osteopetrotic because of the failure in osteoclast differentiation, indicating a crucial role of NF-κB in osteoclastogenesis.[12,13] NF-κB activation requires sequential phosphorylation, ubiquitination, and degradation of the inhibitory subunit IκB as well as consequent exposure of a nuclear localization signal on NF-κB.[14–16] IκB kinase (IKK) signalsome is the protein complex that contains the inducible IκB kinase activity and consists of IKK1 (IKKα), IKK2 (IKKβ), and the NF-κB essential modulator (NEMO

The authors have no conflict of interest.

[1]Department of Sensory and Motor System Medicine, The University of Tokyo Graduate School of Medicine, Tokyo, Japan; [2]Department of Biochemistry and Molecular Biology, The University of Tokyo Graduate School of Medicine, Tokyo, Japan.

or IKKγ). Among these three components of IKK signalsome, both IKK1 and IKK2 seem to play a critical role in IκB phosphorylation. However, the studies of IKK1 and IKK2 knockout mice indicate that IKK2 is more potent for NF-κB activation by proinflammatory stimuli than IKK1.[17–20] This evidence suggests that IKK2 may have a vital function in RANKL-induced NF-κB activation, and in fact, we previously reported that the dominant negative IKK2 ($IKK2^{DN}$) overexpression suppressed both NF-κB activity and osteoclast formation induced by RANKL using the murine monocytic RAW264.7 cell culture.[21]

Proliferation of eukaryotic cells depends on their progression through the cell cycle, and at least a temporal cell cycle arrest at the G1 phase is thought to be a prerequisite for cell differentiation.[22] Cell cycle control is achieved through the actions of a family of cyclins and cyclin-dependent protein kinases (Cdk's), which phosphorylate and thereby activate cell cycle factors essential for the onset of the next cell cycle phase. In mammalian cells, traverse through G1 and subsequent S phase entry require the activities of the cyclin D-dependent kinases Cdk4 and/or Cdk6 and the cyclin E-dependent kinase Cdk2. These Cdk's are negatively regulated by inhibitory proteins (CKIs) through direct binding to themselves.[23,24] CKIs have been classified into two families: INK4 and Cip/Kip. INK4 (p16, p15, p18, and p19) inhibits only Cdk4 and Cdk6, whereas Cip/Kip (p21, p27, and p57) inhibits all the Cdk's except for the Cdk6-cyclin D3 complex.[25] Because the control of cell cycle factors driving S phase onset greatly influences the commitment to cell differentiation in lower eukaryotes, this study investigated the possibility of crucial participation of some cell cycle start factors in RANKL-induced osteoclast differentiation and found that on RANKL treatment Cdk6 was downregulated primarily by RANKL/NF-κB signal-invoked transcriptional repression and that its downregulation was essential for efficient osteoclast differentiation.

MATERIALS AND METHODS

Reagents and antibodies

Human soluble recombinant RANKL was purchased from Wako Pure Chemicals (Osaka, Japan). Recombinant human macrophage-colony stimulating factor (M-CSF) was purchased from R&D Systems (Minneapolis, MN, USA). Antibodies against Cdk2 (H-298), Cdk4 (C-22), Cdk6 (C-21), cyclin D1 (C-20), cyclin D2 (M-20), cyclin D3 (C-16), cyclin E (M-20), p18 (M-20), p27 (F-8), mitogen-activated protein kinase kinase 7 (MKK7; MEK7), and IKK2 (H-470) were purchased from Santa Cruz Biotechnology (Santa Cruz, CA, USA). Antibodies against β-actin (AC-15) were purchased from Sigma Chemical (St Louis, MO, USA). DMEM and FBS were also purchased from Sigma Chemical. αMEM was purchased from Life Technologies (Rockville, MD, USA).

Cell culture and osteoclast differentiation assay

The RAW264.7 cell line was purchased from the Riken Cell Bank (Tsukuba, Japan). The cells were inoculated at 5×10^4 cells in a 6-well plate or 5×10^5 cells in a 10-cm plate and were cultured with DMEM containing 10% FBS at 37°C in 5% CO_2 in air. For osteoclast differentiation assay, RAW cells were grown in DMEM containing 10% FBS for 16–24 h. The culture medium was changed to DMEM containing 0.5% FBS, and the cells were cultured under serum starvation for 24–48 h. The growth-arrested RAW cells were stimulated with 10% FBS in the presence or absence of RANKL (100 ng/ml) for 1–7 days, fixed with 3.7% (vol/vol) formaldehyde in PBS), and stained at pH 5.0 in the presence of L(+)-tartaric acid using 3-hydroxy-2-naphthoic acid 2,4-dimethylanilide phosphate (Sigma) in *N,N*-dimethyl formamide (Sigma) as the substrate. $TRACP^+$ cells containing more than three nuclei were counted as osteoclasts.

For studies on primary osteoclast precursors, we used the M-CSF–dependent bone marrow macrophage (M-BMMϕ) culture system as described previously.[26] Briefly, bone marrow cells from 8-week-old male ddY mice (Sankyo Laboratories Animal Center, Tokyo, Japan) were seeded at 2×10^6 cells in a 6-multiwell plate and cultured in αMEM containing 10% FBS with M-CSF (10 ng/ml). After 2 days, adherent cells were used as M-BMMϕ after washing out the nonadherent cells including lymphocytes. The cells were then cultured in αMEM containing 0.5% FBS for 24 h and were further cultured in the presence of M-CSF (10 ng/ml) and RANKL (100 ng/ml) for 4 days. This experiment was performed according to the protocol approved by the Animal Care and Use Committee of the University of Tokyo.

Western blot analysis

Cells were rinsed with ice-cold PBS and lysed with RIPA buffer (100 μl for a well in 6-multiwell plate or 500 μl for a 10-cm plate) containing 10 mM Tris-HCl (pH 7.5), 150 mM NaCl, 1% Nonident-P40 (NP-40), 0.1% SDS, 10 μg/ml aprotinin, 0.1 M NaF, 2 mM Na_3VO_4, and 10 mM β-glycerophosphate. The cell lysates were sonicated briefly and clarified by centrifugation at 15,000*g* for 20 minutes at 4°C. The protein concentration in the cell lysate was measured using a Protein Assay Kit II (Bio-Rad). Equivalent amounts (10 μg) of cell lysate were electrophoresed by 7.5%, 10%, or 12.5% SDS-PAGE according to the molecular size of the proteins to be detected and were electrotransferred to polyvinylidene difluoride membranes (Immobilon-P; Millipore, Bedford, MA, USA). After blocking nonspecific binding with 5% skim milk, proteins were immunoblotted with respective antibodies and visualized using the ECL Plus Western Blotting Detection System (Amersham Pharmacia Biotech, Buckinghamshire, UK), following the manufacturer's instructions. Signals were quantified by densitometry (Bio-Rad). Experiments were performed at least three times, and a representative blotting was presented.

Transduction of $IKK2^{DN}$ and $MKK7^{DN}$ using adenovirus

The recombinant adenovirus vectors carrying the $IKK2^{DN}$ (Ser177 and Ser181 to Ala; $AxIKK2^{DN}$) and the *β-galactosidase* gene (AxLacZ) were kindly provided by Inder Verma (Salk Institute, La Jolla, CA, USA) and Izumu Saito (Tokyo University), respectively. The recombinant

adenovirus vector carrying kinase negative MKK7 ($AxMKK7^{DN}$, replaced ATP-binding lysine with glutamate residue) was constructed as described.[21] Preparation and infection of $AxIKK2^{DN}$, $AxMKK7^{DN}$, and AxLacZ were performed as previously reported.[21] Titers of the viral stock were determined by modified endpoint cytopathic effect assay with the following modifications. Fifty microliters of DMEM containing 10% FBS was dispensed into each well of a 96-well tissue culture plate, and eight rows of 3-fold serial dilutions of the virus starting from 10^{-4} dilutions were prepared. HEK293 cells (3×10^5) in 50 μl of DMEM containing 10% FBS were added to each well. The plate was incubated at 37°C in 5% CO_2 in air, and 50 μl of DMEM containing 10% FBS was added to each well every 3 days. Twelve days later, the endpoint of the cytopathic effect was determined by microscopy, and the 50% tissue culture infectious dose ($TCID_{50}$) was calculated. One $TCID_{50}$ per milliliter approximately corresponds to one plaque-forming unit (PFU) per milliliter. The multiplicity of infection (MOI) is expressed as a measure of titer of how many PFUs are added to every cell. Infection of adenovirus vectors to RAW cells was carried out as follows. The cells were inoculated at the density of 5×10^4 cells per 6-well plate and incubated for 20 h with DMEM containing 10% FBS at 37°C. After further incubation with a small amount of DMEM containing the recombinant adenovirus for 2 h at 37°C at 100 MOI, the cells were washed twice with PBS and again incubated in DMEM containing 10% FBS. Experiments were performed 2 days after the infection.

Establishment of RAW cells stably transfected with Cdk6

RAW cells were inoculated at the density of 5×10^5 cells per 6-cm plate, incubated for 24 h, and transfected with pEF/neoI that carries human *Cdk6* cDNA[25] using LipofectAMINE reagent (Life Technologies) following the manufacturer's instructions. Twenty-four hours after transfection, the cells were passaged 1:10–1:100 into DMEM containing 10% FBS and 400 μg/ml G418 (Geneticin; Life Technologies) for stable expression. After colony formation, each colony was isolated and passaged. We picked up more than 100 drug-resistant colonies, each of which was derived from a single clone. The expression levels of Cdk6 were quantified by Western blotting, and 12 high-expressing clones and 10 low-expressing clones were established.

RT-PCR

Total RNA (1 μg) was extracted from RAW cells using ISOGEN (Wako Pure Chemicals, Osaka, Japan) following the manufacturer's instructions, reverse transcribed using SUPERSCRIPT First-Strand Synthesis System for RT-PCR (Life Technologies), and amplified within an exponential phase of the amplification with a Perkin Elmer PCR Thermal Cycler (PE-2400). Gene-specific primer pairs were as follows: 5′-GCAACCTCCAGTCAGCA-3′ and 5′-GAAGTCACAGCCCTCAGAATC-3′ for RANK and 5′-CATGTAGGCCATGAGGTCCACCAC-3′ and 5′-TGAAGGTCGGTGTGAACGGATTTGGC-3′ for GAPDH. The cycling parameters were 30 s at 94°C, 30 s at 49°C, and 90 s at 72°C for RANK and 30 s at 94°C, 30s at 55°C, and 90 s at 72°C for GAPDH. Each band intensity was quantified by densitometry (Bio-Rad).

Flow cytometric analysis

About 1×10^5 cells were suspended in 0.02 ml citrate buffer, to which was added 0.18 ml Soln. A (0.03 mg/ml trypsin, 3.4 mM trisodium citrate, 0.1% NP40, 1.5 mM Spermine 4 HCl, and 0.5 mM Tris-HCl [pH 7.6]) and incubated for 10 minutes, and then added with 0.15 ml Soln. B (3.4 mM trisodium citrate, 0.1% NP40, 1.5 mM Spermine 4 HCl, 0.5 mM Tris-HCl [pH 7.6], 0.5 mg/ml trypsin inhibitor, 0.1 mg/ml Ribonuclease A) and incubated for 10 minutes; 0.15 ml Soln. C (4.16 mg/ml propidium iodite, 3.4 mM trisodium citrate, 0.1% NP40, 4.8 mM Spermine 4 HCl, 0.5 mM Tris-HCl [pH 7.6]) was finally added, and the mixture was again incubated for 10 minutes. All procedures were performed at room temperature. The DNA content was analyzed by EPICS XL (Beckman), and the data were analyzed by XL EXPO32 (Beckman).

BrdU incorporation assay

RAW cells were inoculated at a density of 1×10^3 cells per well in a 96-well plate and cultured in DMEM containing 10% FBS with or without hRANKL (100 ng/ml). At 3 days of culture, cells were labeled with BrdU for 2 h, and cell proliferation was determined by BrdU incorporation using a kit (Cell Proliferation ELISA; Roche Molecular Biochemical, Mannheim, Germany) following the manufacturer's instructions.

Statistical analysis

Means of groups were compared by ANOVA, and significance of differences was determined by posthoc testing using the Bonferroni method.

RESULTS

Cdk6 is downregulated by RANKL in RAW cells

We initially confirmed that RAW cells differentiated into $TRACP^+$ multinucleated osteoclasts after 5 days of treatment with soluble RANKL (100 ng/ml; Fig. 1A). We analyzed the regulation by RANKL of cell cycle factors that critically regulate the onset of S phase: Cdk2, Cdk4, Cdk6, cyclins (D1, D2, D3, and E), and CKIs (p18, p21, and p27) in RAW cells (Figs. 1B and 1C). Western blot analysis revealed that the Cdk6 protein level was decreased by RANKL after 5 days of culture and thereafter, whereas those of cyclins were hardly affected throughout the culture period up to 7 days. Although Cdk4 and Cdk6 have about 70% homology of amino acid sequence[27] and share D cyclins as their catalytic partners, only Cdk6 was regulated by RANKL. Levels of Cdk2, p18, and p27 were somewhat decreased by RANKL treatment, and neither p21 nor p57 was detected throughout the experiments in this cell line (data not shown).

To investigate whether the Cdk6 downregulation is specific to this cell line or a more general phenomenon, we performed the same Western blot analysis with a culture of

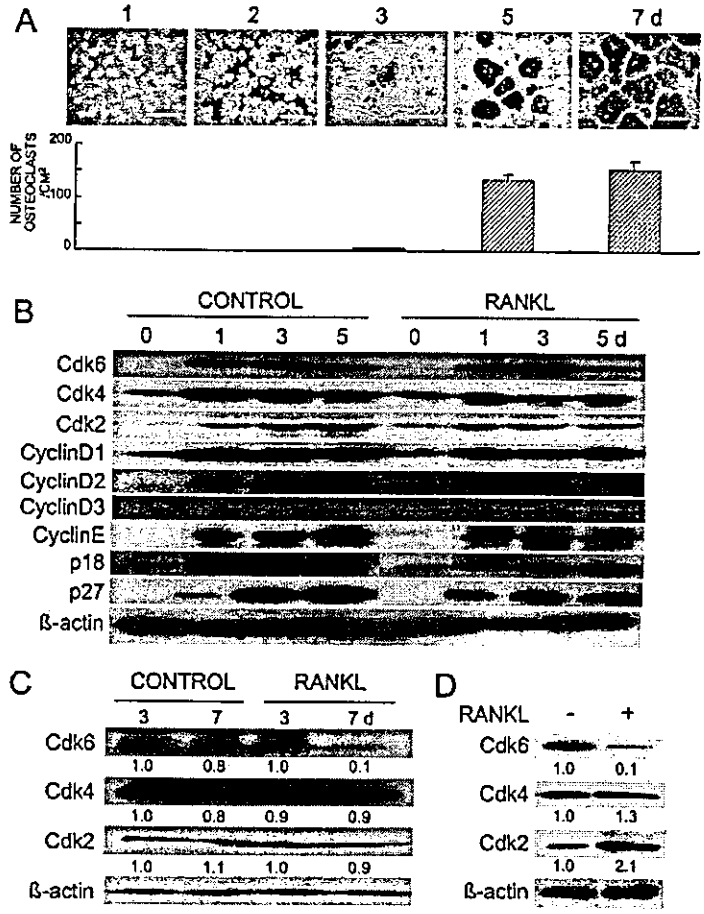

FIG. 1. (A) Time course of osteoclastogenesis from murine monocytic RAW264.7 cells, (B and C) expression of cell cycle factors by RANKL in the RAW264.7 cell culture, and (D) the murine primary osteoclast precursor M-BMMϕ culture. Cells were stimulated with serum in the presence or absence of RANKL (100 ng/ml) for the indicated days. (A) Osteoclastogenesis formed from cultured RAW cells was determined by TRACP staining, and the number of positively stained cells containing more than three nuclei was counted. Bar, 400 μm. The graph is expressed as means (bars) ± SE (error bars) for 8 wells/group. (B–D) The protein levels of cell cycle factors controlling the G1-S transition were determined at the indicated days of culture by Western blot analysis. β-actin was used as a loading control. B and C are from different cultures of RAW cells to confirm the regulation of Cdk's. D is from the M-BMMϕ culture for 4 days. The number under each band is the treated/control ratio of the intensity of each band normalized to that of β-actin measured by densitometry. In each figure a representative blotting was shown among at least three independent experiments that showed similar results.

primary osteoclast precursor M-BMMϕ. Treatment with RANKL inhibited induction of Cdk6 at 4 days, whereas Cdk4 was uninfluenced (Fig. 1D). Cdk2 was not decreased but was rather increased in this culture system. These results show that Cdk6 was specifically downregulated during the commitment to RANKL-induced osteoclast differentiation.

NF-κB mediates RANKL-induced downregulation of Cdk6

To examine the mediation of the NF-κB pathway, a major signaling pathway of RANKL, in the downregulation of Cdk6, we overexpressed $IKK2^{DN}$ in RAW cells using an adenovirus vector and examined its effect on RANKL-led Cdk6 downregulation. In our previous report, we confirmed that the adenovirus vector could efficiently transduce the $IKK2^{DN}$ gene into RAW cells and specifically suppressed the NF-κB activation in response to RANKL.[21] Both the inhibition of Cdk6 and the induction of osteoclastogenesis by RANKL were markedly reversed by the $IKK2^{DN}$ overexpression in RAW cells, whereas the control LacZ adenovirus infection did not affect the RANKL actions (Fig. 2A). These results indicate that the NF-κB signaling mediates not only osteoclast differentiation, but also the Cdk6 downregulation by RANKL.

We further investigated the possible involvement of the c-*jun* N-terminal kinase (JNK), another major signaling pathway of RANKL, in the downregulation of Cdk6 by RANKL. We previously reported that MKK7 is a vital function in JNK activation and osteoclast formation induced by RANKL, because $MKK7^{DN}$ overexpression using an adenovirus vector suppressed both of them.[21] Thus, we examined the effect of the adenovirus-mediated $MKK7^{DN}$ overexpression on RANKL-led Cdk6 downregulation in RAW cells. The $MKK7^{DN}$ overexpression suppressed the induction of osteoclastogenesis by RANKL as previously reported[21]; however, it did not restore the inhibition of Cdk6 in response to RANKL, unlike $IKK2^{DN}$ overexpression (Fig. 2B), indicating that the RANKL-led Cdk6 downregulation was not mediated by the JNK signaling.

RAW cells overexpressing Cdk6 resist RANKL-induced differentiation

As shown above, Cdk6 downregulation occurred during RANKL-induced osteoclast differentiation. Consequently, a critical question is whether or not this downregulation is essential for osteoclast differentiation. To address this, we generated RAW cell clones stably expressing various levels of Cdk6 by transfecting with an expressing vector harboring